Heliyon 10 (2024) e27976

Contents lists available at ScienceDirect

Heliyon

journal homepage: www.cell.com/heliyon

Research article

Mapping the 5-HTergic neural pathways in perimenopausal mice and elucidating the role of oestrogen receptors in 5-HT neurotransmission

Hanfei Wang [a], Yanrong Sun [a], Wenjuan Wang [a], Xiangqiu Wang [a], Jinglin Zhang [b], Yu Bai [a], Ke Wang [a], Liju Luan [a], Junhao Yan [a], Lihua Qin [a,*]

[a] *Department of Human Anatomy, Histology and Embryology, School of Basic Medical Sciences, Peking University Health Science Center, Beijing, 100191, China*

[b] *Department of Dental Medicine, School of Dental Medicine, Yuncheng Vocational Nursing College, Yuncheng, 044000, China*

ARTICLE INFO

Keywords:
Perimenopause
5-HT
Neural pathway
Oestrogen receptors
Hot flashes

ABSTRACT

Perimenopausal syndrome (PMS) encompasses neuropsychiatric symptoms, such as hot flashes and depression, which are associated with alterations in the 5-HTergic neural pathway in the brain. However, the specific changes and mechanisms underlying these alterations remain unclear. In this study, ovariectomized mice were used to successfully establish a perimenopause model, and the changes in the expression of 5-HT and its receptors (5-HT1AR and 5-HT2AR) across 72 brain regions in these ovariectomized mice were assessed by immunohistochemistry. Although both 5-HT and 5-HT1AR were widely expressed throughout the brain, only a limited number of regions expressed 5-HT2AR. Notably, decreased expression of 5-HT was observed across almost all brain regions in the ovariectomy (OVX) group compared with the Sham group. Altered expression of both receptors was found within areas related to hot flashes (the preoptic area) or mood disorders (the amygdala). Additionally, reduced oestrogen receptor (ER)α/β expression was detected in cells in the raphe nucleus (RN), an area known to regulate body temperature. Results showed that ERα/β positively regulate the transcriptional activity of the enzymes TPH2/MAOA, which are involved in serotonin metabolism during perimenopause. This study revealed the changes in 5-HT neuropathways (5-HT, 5-HT1AR and 5-HT2AR) in perimenopausal mice, mainly in brain regions related to regulation of the body temperature, mood, sleep and memory. This study clarified that the expression of oestrogen receptor decreased in perimenopause, which regulated the transcription levels of TPH2 and MAOA, and ultimately led to the reduction of 5-HT content, providing a new target for clinical diagnosis and treatment of perimenopausal diseases.

1. Introduction

As ovarian function gradually fails, various symptoms related to different body systems develop, and these symptoms include hot flashes, depression, insomnia, and impairments in learning and memory. These symptoms are collectively known as perimenopausal syndrome (PMS) [1]. Among these symptoms, hot flashes are the specific symptom of menopause and indicate a high incidence of

* Corresponding author.
E-mail address: qinlihua88@bjmu.edu.cn (L. Qin).

https://doi.org/10.1016/j.heliyon.2024.e27976
Received 11 August 2023; Received in revised form 7 March 2024; Accepted 8 March 2024
Available online 11 March 2024

cardiovascular disease. Oestrogen and neurotransmitter modulators, such as selective serotonin reuptake inhibitors (SSRIs), can effectively relieve these symptoms [2,3]. However, these agents have many side effects, including but not limited to breast cancer, stroke, and serotonin syndrome [4,5]. As a result, the treatment of PMS is challenging. Exploring the roles of oestrogen and serotonin (5-HT) in the central nervous system and finding new effective intervention targets for clinical treatment will help us overcome these problems.

Hot flashes are part of abnormal body thermoregulation. 5-HT and its receptors (5-HT1AR and 2AR) play roles in thermoregulation [6]. The injection of 5-HT into the cisterna magna increases the body temperature [7]. When 5-HT1AR and 5-HT2AR are activated in the preoptic area, effectors mediate heat dissipation and production, respectively [6]. However, whether these genes are also involved in perimenopausal hot flashes is unclear. Our previous work revealed that the distribution of 5-HTergic nerve fibres, 5-HT1AR and 5-HT2AR in the hypothalamic preoptic area (POA), the central thermoregulatory centre, is significantly altered in ovariectomized rats [8]. These results suggest that the alterations in 5-HTergic neural pathways after OVX may be involved in perimenopausal hot flashes. Moreover, 5-HT and its receptors play key roles in the development of depression [9]. 5-HT1AR and 5-HT2AR are the targets of many antipsychotic drugs [10,11]. In women, emotional symptoms triggered by oestrogen level alterations may be related to alterations in the 5-HTergic neural pathway [10], but evidence of the underlying mechanism is lacking. In addition, 5-HT and its receptors are associated with circadian rhythms. The serotonergic system promotes sleep in both diurnal zebrafish and nocturnal rodents [12], whereas 5-HT deficiency in the adult brain leads to hyperactivity, circadian disruption, and an inability to sleep during the day [13]. Agonists or inhibitors of 5-HT1AR and 5-HT2AR can regulate the sleep phase of the sleep–wake cycle and treat insomnia [14,15]. Moreover, 5-HT and its receptors are associated with learning and memory [16]. 5-HT deficiency alters hippocampal synaptic plasticity, affecting the memory capacity [17]. 5-HT1AR is involved in the response to temporal memory [18], and 5-HT1AR expression is reduced in the hippocampus of patients with Alzheimer's disease (AD) [19]. The abovementioned evidence suggests that 5-HT and its receptors in the brain regulate physiological functions. How the expression of 5-HT and its receptors is altered in various brain regions during perimenopause and whether the occurrence of PMS (such as hot flashes) is associated with such changes are unclear. Although information about receptor expression in the whole brain of male mice is available at http://portal.brain-map.org/, the changes in the expression of relevant receptors that occur in the brains of female mice and ovariectomized mice remain unknown.

5-HTergic neurons in the brain are concentrated in the raphe nucleus (RN) and account for two-thirds of the total neurons in the RN [20]. The axons of these cells innervate most brain regions and primarily express 5-HT1AR and 5-HT2AR [21]. 5-HT is synthesized by the key enzyme tryptophan hydroxylase (TPH2) and then degraded by monoamine oxidase A (MAOA) [22]. Therefore, TPH2 and MAOA affect the content of 5-HT in the RN. In the perimenopausal period, prolonged low oestrogen levels lead to oestrogen receptor (ER) exhaustion in the brain [23]. Several studies have revealed the regulatory effect of ERβ on TPH2 [24,25], but little is known about the effect of ERα on enzymes related to 5-HT metabolism. We hypothesize that ERα and ERβ act as transcription factors to affect the 5-HT levels by regulating the transcription and translation of 5-HT metabolism-related enzymes, such as TPH2 and MAOA, thus altering the expression of 5-HT receptors in related brain regions to trigger PMS symptoms, such as hot flashes.

To confirm this speculation, the expression of 5-HT and its receptors (5-HT1AR and 5-HT2AR) in the brains of ovariectomized mice and normal female mice was assessed and mapped. We detected ER and other 5-HT anabolism-related molecules in the RN after OVX. The target genes associated with 5-HT metabolism bound by the nuclear oestrogen receptor in the RN were identified by CUT&Tag. The expression of these target genes identified by screening was verified by a dual-luciferase assay and stereotaxic injections of activors and depressors, and the body temperature changes were monitored. In this study, we revealed the changes in 5-HTergic neural pathways in the brains of mice after OVX; explored the mechanisms underlying these changes, specifically those involving nuclear oestrogen receptors that act as transcription factors; and performed screening to validate the identified molecular targets related to 5-HT metabolism.

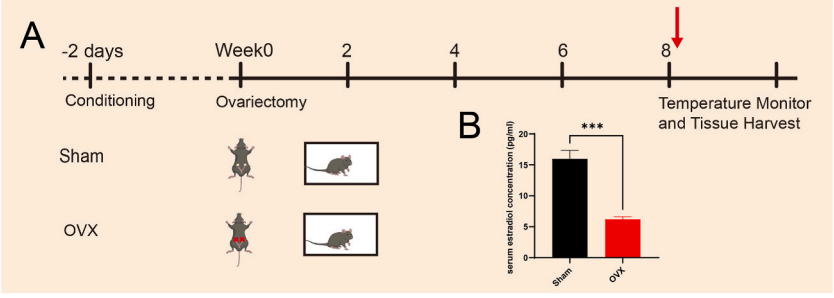

Fig. 1. OVX procedure and verification in mice. **(A)** Diagram of the procedure used for animal model construction. The mice were divided into 2 groups, and only the ovaries of those in the OVX group were removed. After eight weeks, the behavioural phenotype was observed, and specimens were harvested. (**B**) Oestradiol levels in the serum of arteriovenous mixed blood; n = 11 biologically independent animals per group. The data are shown as the means ± SEMs. Student's *t*-test was used to analyse the differences between the two groups; ***$P < 0.001$.

2. Materials and methods

2.1. Construction of an OVX mouse model

Eight-week-old female C57BL/6J mice weighing 17 ± 1 g were purchased from the Laboratory Animal Science Department of Peking University Health Science Center. The animals were housed in the laboratory with a temperature of 25 ± 2 °C and a relative humidity of 40–50% under a 12-h light/dark cycle. The mice were given free access to water and soy-free food to exclude the effects of soy isoflavones. The study was performed with the approval of the local ethics committee, and the animal experiments were approved by the Laboratory Animal Welfare Ethics Branch, Biomedical Ethics Committee, Peking University. Approval No. LA2022429.

The mice (n = 105) were randomly divided into two groups: Sham and OVX groups. OVX was performed through a single incision via a dorsal approach, and the animals were anaesthetized with 1.25% tribromoethanol at a dose of 0.02 ml/g. A 1.5-cm incision was made at the back of the costal arch, and the ovaries were located by dissecting the underlying adipose tissue (Supplementary Fig. 1A). The ovaries were then ligated with 5–0 silk thread to achieve OVX (n = 50). The mice in the Sham group were subjected to the same procedure except for the ligation and excision (n = 65). The mice in the Sham and OVX groups were observed after postoperative recovery and treated with furacilin if necessary. The animals were kept alone in a cage for 8 weeks. Therefore, the modeled Sham and OVX group used below are 4 months old.

2.2. Assessment of successful OVX animal model construction

After OVX, the back incision was monitored for infection. Eight weeks later, the vagina was irrigated at a fixed time for 5 days. Haematoxylin and eosin (HE) staining was performed to confirm that the mice in the Sham group experienced a regular oestrous cycle, whereas those in the OVX group exhibited no oestrous cycle. Mice that did not meet these criteria were discarded. According to the morphology of the shed vaginal cells, all tissue samples (including blood serum, brain tissue, uterus and ovary) from the Sham group were obtained during the oestrous phase. The oestrogen levels increase during the proestrus phase and peak during the oestrous phase. This time point best represents the normal physiological state of nonperimenopausal mice. Tissue sample collection was then conducted. The animals were anaesthetized as described above, and arteriovenous blood was collected from the orbital sinus. After the blood was allowed to clot at room temperature for 30 min and centrifuged at 4 °C and 2500 rpm for 10 min, the supernatant was frozen at −80 °C, and the oestradiol levels were measured with an enzyme-linked immunosorbent assay (ELISA) kit (Furuirunze, Beijing). Thereafter, tissue samples (ovary, uterine and whole-brain tissue) were collected and perfused with fixative to assess the presence and morphology of the ovaries. All animal models were confirmed by staining of vaginal exfoliated cells and abdominal laparotomy.

2.3. Measurement of the skin temperature in OVX model animals

Eight weeks after successful OVX, we randomly selected 13 mice from each group (Sham and OVX) for measurement of the body surface temperature while the mice were awake rather than under anaesthesia. The measurements were conducted in the afternoon for 5 consecutive days. According to research conducted by Yu Sun, the surface temperature of the mice in the OVX group reaches its peak in the afternoon [26], and the difference in body surface temperature between the Sham and OVX groups was greater during this period. Moreover, the ambient temperature tends to increase during the afternoon, which facilitates observation of the differences between groups. The mice were placed in a 20-cm^3 open foam box in which they could move freely, and their skin temperature was continuously monitored for 10 min. An infrared thermal imager (FOTRIC) was placed on top of the foam box to ensure an ambient temperature of 26 ± 1 °C. The average temperature of the specific skin area was calculated using AnalysIR thermal image analysis software.

2.4. Immunohistochemistry (IHC) and image analysis

After staining of vaginal exfoliated cells and ethological tests (body temperature), the mice were anaesthetized as described above, and 5 mice were randomly selected from each group (Sham and OVX). NaCl (0.9%) and 4% paraformaldehyde (PFA) were successively injected into the left ventricle of each mouse, after which a small incision was made into the right atrium. The liquid was moved through the systemic circulation to achieve blood expulsion and protein fixation and to preserve whole-body tissues and organs. The brain and spinal cord were subsequently separated from the foramen magnum. The brain tissues were harvested, placed in 4% PFA for 6 h for postfixation and soaked in 20% or 30% sucrose (0.1 M phosphate buffer solution as a solvent) until they sank. The brain tissues were embedded in optimal cutting temperature (OCT) compound, flash frozen in liquid nitrogen and subsequently stored at −80 °C. The whole brains of five mice per group were cut at a thickness of 50 μm. Six sets of brain slices were placed in antifreeze solution. To label 5-HTergic neurons and fibres, the slices were incubated in 1% Triton X-100 for 4 h and citrate buffer at 95 °C for 15 min, subjected to three 5-min washes with phosphate buffer solution (PBS), rinsed with 3% H_2O_2 at room temperature for 30 min, and subjected to three 50min washes with PBS. The slices were blocked with 5% goat serum for 1 h, incubated with an anti-5-HT primary antibody (ab6336; Abcam) (1:100) for 96 h, subjected to three 5-min washes with PBS, incubated with a secondary antibody (PV9004; ZSGB-BIO) at room temperature for 100 min, stained with 3,3 N-diaminobenzidine tetrahydrochloride (DAB) (1 ml of Reagent A and 1 drop of Reagent B) at room temperature for 30 min, and transferred to PBS for mounting. For the staining of whole brains for 5-HT1AR and 5-HT2AR, the slices were rinsed with 1% Triton X-100 at room temperature for 1 h, incubated with anti-5-HT1AR (NBP2-21590, Novus) (1:800) and anti-5-HT2AR primary antibodies (Ab66049, Abcam) (1:800) for 16 h, incubated with a secondary antibody

(SP9001, ZSGB-BIO) for 120 min at room temperature and stained with DAB (prepared as described above) for 2 min at room temperature. The stained brain slices were mounted on cation anti-stripping slices (ZLI-9506, ZSGB-BIO) for gradient dehydration and sealing. After being dehydrated with graded alcohol solutions and cleared in xylene, the slices were sealed with xylene and neutral gum. All the antibodies used in this study are listed in Table 1. Panoramic slice scanning was performed using a pathology slice scanning instrument (WS-10, WISLEAP). NDP. View 2 software was used to obtain images.

Previous studies have classified mouse whole-brain slides into distinct regions, namely, the telencephalon, diencephalon, mesencephalon, metencephalon, and myelencephalon [27]. Within each specific brain region, the extent of 5-HTergic nerve fibre innervation observed by Aude Muzerelle using virus tracing technology was further validated [28]. The subnuclei of interest were identified based on coronal sections of the fourth edition of Paxinos and Franklin's Mouse Brain in Stereotaxic Coordinates [29] and magnified 80× with a unit area of 27,500 μm^2 to ensure a consistent image background. Three images were selected from each brain region of 5 mice for analysis, and Image-Pro Plus software was used to calculate the number of positive cells and the optical density per unit area (average optical density, AOD). A cell exhibiting complete morphology with DAB staining was considered an individual cell entity, and a connected line in a cross-section represented a fibre.

2.5. Stereotaxic injection of ERα and ERβ activators and depressors into the RN

Erα and Erβ activators and depressors were injected into the RN of ovariectomized animals at the following coordinates: +4.7 mm AP, 0 mm ML, and +4.0 mm DV. Two groups (n = 15 per group) were generated (the animal model is now four months old): mice in the OVX group injected with an ERα activator (O-ERα-A) and in the OVX group injected with an ERβ activator (O-ERβ-A). Similarly, ERα and ERβ depressors or solvent were injected into the RN of Sham animals in two groups (n = 15 per group): mice in the Sham group injected with an ERα depressor (S-ERα-D) and mice in the Sham group injected with an ERβ depressor (S-ERβ-D). The product numbers, concentrations and dosage of the four drugs, as well as associated references, are listed in Table 2. The drug solvent consisted of 10% DMSO, 40% PEG300, 5% Tween-80, and 45% saline according to the instructions of MedChemExpress. Each mouse was injected with 2 μl of drug via a microinjector (7632–01, Hamilton). All drugs and solvents were purchased from MedChemExpress. After brain stereotaxic surgery, the mice were housed individually and kept in a warm environment to ensure successful recovery. The body temperature was measured 3 days after stereotaxic surgery as described above, and brain tissues were collected from the RN (refer to the Western blotting section for details). From each group of 15 mice, 5 samples were used to detect the 5-HT and MAOA protein concentrations via ELISA, 5 samples were used to detect the TPH2 and MAOA in protein expression level via WB (the antibodies used are listed in Table 1), and 5 samples were used to detect the TPH2 and MAOA in RNA expression level via qPCR (the primers used are listed in Table 3, the primer sequence was designed by RuiBiotech company). Mouse ELISA kits were used to measure the concentrations of 5-HT (RJ-113, Furuirunze) and MAOA (QS48397, Qisong) in the RN according to the manufacturer's instructions.

2.6. Western blotting (WB)

Five mice were randomly selected from the Sham, OVX, S-ERα-D, S-ERβ-D, O-ERα-A and O-ERβ-A groups. The procedure for obtaining fresh mouse brain tissue from the RN was as follows: After the mice were anaesthetized with tribromoethanol, their brain tissues were rapidly dissected and removed, and residual blood was washed away with PBS precooled at 4 °C. The brains were placed in a mould, cut with a blade adjacent to the RN (AP: 4.0 to −5.3 mm, ML: ±0.75 mm, DV: +2.5–5 mm), flash frozen in liquid nitrogen, and subsequently stored at −80 °C. The tissues were ground in RIPA buffer (C1053+, Applygen) containing phosphatase inhibitor and protein protease inhibitor (P1265, Applygen) with a homogenizer and centrifuged in a precooled centrifuge. The supernatant was retained, and the sediment was discarded. The protein concentration was quantified with a BCA kit (P1511-2, Applygen). The proteins were prepared for loading, and the protein concentrations were adjusted with loading buffer. A total of 20 μg of each sample was loaded on a 10% SDS–PAGE gel (WB1102, Biotides), and the proteins were separated in 1 × electrophoresis buffer at 80 V for 120 min. The proteins were then transferred to a polyvinylidene difluoride (PVDF) membrane at 100 V for 100 min. Subsequently, the PVDF membrane was incubated with 5% milk powder (P1022-500, Applygen) for 1 h, washed with Tris-buffered saline (TBS) for 5 min, incubated with primary antibody (see Table 1) in TBST (tris-buffered saline supplemented with Tween-20) 3 times for 10 min each, incubated with secondary antibody, washed 3 times with TBST, and developed using Super ECL solution (P1010-250, Applygen). GAPDH (C1312, Applygen) was used as an internal reference gene. All the antibodies used in this study are listed in Table 1. The

Table 1
Primary antibodies used in this study.

Primary antibody	Catalogue number	Antibody brand	Dilution
Rat anti-mouse serotonin antibody	ab6336	Abcam	1:100 (IHC)
Rabbit anti-mouse 5-HT1A receptor antibody	NBP2-21590	Novus	1:800 (IHC)
Rabbit anti-mouse 5-HT2A receptor antibody	ab66049	Abcam	1:800 (IHC)
Rabbit anti-mouse ERα antibody	A12976	ABclonal	1:1000 (WB)
Rabbit anti-mouse ERβ antibody	bs-0116R	Bioss	1:1000 (WB)
Rabbit anti-mouse GPR30 antibody	bs-1380R	Bioss	1:1000 (WB)
Rabbit anti-mouse MAOA antibody	A1354	ABclonal	1:1000 (WB)
Rabbit anti-mouse TPH2 antibody	A14520	ABclonal	1:1000 (WB)
Mouse anti-mouse GAPDH antibody	C1312	Applygen	1:1000 (WB)

Table 2
Stereotaxic injection of ERα and ERβ activators and depressors into the RN.

Drug effect	Drug	Catalogue number	Concentration (mg/ml)	Dosage (mg/kg body weight)	Reference
ERα activator	Propyl pyrazole triol	HY-100689	10	1	[61]
ERα depressor	AZD9496	HY-12870	10	1	[62]
ERβ activator	Liquiritigenin	HY-N0377	75	7.5	[63]
ERβ depressor	PHTPP	HY-103456	10	1	none

Table 3
Primers used for qPCR in this study.

	Forward primer (5′-3′)	Reverse primer (5′-3′)
ERα	GCCCTACTACCTGGAGAACG	ACAGTCTCTCGGCCATTC
ERβ	AGACTGCAAGCCCAAATGTG	TTTGAGGTTCTGCATAGAGA
GPR30	TGGCCCTCAACTTGTCCCTG	CCACCAGGATGAGGATGTTG
MAOA	ATAGAGTTGGAGGAAGAA	TAGACAAGCGTAAGATTC
TPH2	AGTTGGTGGGCTGGTGAAAG	GCTCTCAGGCGGATTCAGGG
GAPDH	AGTATGACTCCACTCACGGC	ACCAGTAGACTCCACGAC

relative grey values of the bands were analysed and calculated with ImageJ software.

2.7. RNA extraction followed by qPCR

Five mice were randomly selected from the Sham, OVX, S-ERα-D, S-ERβ-D, O-ERα-A and O-ERβ-A groups. RNA was extracted from the RNA samples with a TransZol Up Plus RNA Kit (ER501-01, Transgene), and the RNA concentration and A260/A280 ratio of each sample were measured to determine the RNA quality. After reverse transcription of RNA into cDNA by a TransScript Uni All-in-One First-Strand cDNA Synthesis Kit (AU341-02, Transgene) and SuperMix for qPCR (One-Step gDNA Removal) (AQ602-22, Transgene), primers specifically targeting ERα, ERβ, GPR30, TPH2, and MAOA were added. RNA expression was detected by a SYBR Green PCR system. The comparative CT method was utilised to calculate the relative mRNA expression levels using GAPDH as the internal reference gene. All the target genes and reference genes and the sequences of the primers used are listed in Table 3.

2.8. CUT&Tag

We randomly selected 15 brain tissue samples from the Sham group. The brain tissue was placed in a homogenizer, reagents from a nuclear extraction kit (Solarbio, SN0020) were added, and the tissue was ground to prepare a single-cell suspension. Fifty microliters of the cell suspension was removed, 10 μl of DAPI solution was added for 1 min, and the cells were observed under a fluorescence microscope to ensure that most of the cells were dissociated and undamaged. The number of DAPI-stained cells was counted, and the number of cells in each 1.5-ml Eppendorf tube was adjusted to more than approximately 100,000 nuclei. Six tubes were used in the following experiments to identify the target gene affected by the transcription factor (ERα and ERβ for the double replication experiments). CUT&Tag was performed with a kit purchased from Novezan Vazyme (TD903). Primary antibodies against ERα (Abcam, ab32063), ERβ (Novus, NB200-305), and histone 3 (#4620, Cell Signaling Technology) and IgG (A7016, Beyotime) were mixed with the Tn5 enzyme from the kit, and the secondary antibody was added to determine the DNA sequence. Sequencing was completed by Novo Gene Company. The sequencing results were subsequently analysed.

2.9. Cell culture, plasmid construction and luciferase assay

SY5Y human neuroblastoma cells (kindly provided by Dr. Chunhua Chen, Peking University) were used. SY5Y cells were cultured in DMEM supplemented with 10% FBS and antibiotics. Candidate sequences were obtained by CUT&Tag. Two pCDNA3.1 (+) plasmids expressing the transcription factors ESR1 and ESR2 and six PGL3-promoter plasmids expressing the binding sites of interest were constructed. The original luciferase plasmid with only TK was used as the control. All the constructed sequences and the sequences of the primers used are listed in Supplementary Table 4. The plasmids were extracted with a HighPure Maxi Plasmid Kit (Tiangen, DP116). The cells were then cotransfected with pRL-TK (as a reference plasmid), pCDNA3.1 (+) and the pGL3 promoter. Luciferase assays were performed with three independent groups of transfected cells using a Dual-Glo Luciferase Assay Kit from Genomeditech. The absorbance was measured by an enzyme marker (Molecular Devices), and the Luc/Rena value was calculated for each plasmid. The original luciferase plasmid with only TK was used as the control. The TLuc/Rena values of the plasmid-expressed transcription factor and promoter action site sequences were measured and calculated as luciferase activity.

2.10. Statistics and analysis

The number of neurons positive for each target protein and the number of nerve fibres were determined. All experimental data are

Table 4
Abbreviations in this study.

Brain region	Abbreviation
Nucleus accumbens	acb
Anterior hypothalamic area	AHA
Amygdalohippocampal nucleus	AHi
Anterior olfactory nucleus	AON
Arcuate nucleus	Arc
Basal nucleus (Meynert)	B
Basolateral amygdaloid nucleus	BLA
Basomedial amygdaloid nucleus	BMA
Bed nucleus of the Stria terminalis	BSTN
CA1	CA1
CA2	CA2
CA3	CA3
Cerebellum	Cb
Central nucleus of amygdala	CeA
Central medial thalamic nucleus	CM
Cortical nucleus of amygdala	CoA
Dentate gyrus	DG
Lateral geniculate nucleus	DLG
Dorsomedial nucleus	DM
Dorsomedial tegmental area	DMTg
Entorhinal cortex	Ent
External plexiform layer	Epl
Habenular commissure	Hbc
Horizontal limb	HDB
Intercalated nuclei of the amygdala	I
Island of Calleja	ICj
Inferior olive	IO
Interpeduncular nucleus	IP
Lateral (dentate) cerebellar nucleus	Lat
Layer 6	Layer 6
Layers 2-3	Layers 2-3
Layers 4-5	Layers 4-5
Locus coeruleus	LC
Laterodorsal tegmental nucleus	LDTg
Laterodorsal thalamic nucleus	LDVL
Lateral hypothalamus	LH
Lateral Parabrachial nuclei	LPB
Lateral preoptic area	LPO
Lateral reticular nucleus	LRt
Lateral septal nucleus	LS
Medial nucleus of amygdala	MePV
Medial mammillary nucleus	MnM
Median preoptic nucleus	MnPO
Medial preoptic area	MPA
Medial Parabrachial nuclei	MPB
Medial septal nucleus	MS
Vascular organ of the lamina terminalis	OVLT
Paraventricular nucleus	Pa
Periaqueductal grey	PAG
Parabrachial nucleus	PB
Posterodorsal tegmental nucleus	PDTg
Periventricular hypothalamic nucleus	Pe
Piriform cortex	Pir
Pontine nuclei	Pn
Posterior thalamic nuclear group	Po
Preoptic area	POA
Retrochiasmatic area	RCh
Raphe nucleus	RN
Subiculum	S
Suprachiasmatic nucleus	SCh
Pars compacta	SNC
Substantia nigra, reticular part	SNR
Superior olive	SO
Nucleus of the solitary tract	Sol
Supraoptic nucleus	SoN
Spinal trigeminal nucleus	SPN
Subthalamic nucleus	STh
Tenia tecta	TT

(*continued on next page*)

Table 4 (*continued*)

Brain region	Abbreviation
Olfactory tubercle	Tu
Vertical limb	VDB
Ventromedial hypothalamic nucleus, dorsomedial part	VMHDM
Ventromedial hypothalamic nucleus, ventrolateral part	VMHVL
Ventral tegmental nucleus	VTg
Zona incerta	ZI

shown as the means ± SEMs. GraphPad Prism 9 was used for data analysis, and $P < 0.05$ was considered to indicate statistical significance. The CUT&Tag data were analysed and processed by the Vazyme cloud platform and Novogene Source software. The location of each site in the promoter region of the gene was determined with SnapGene 6.1.1.

3. Results

3.1. Successful construction of the OVX mouse model

The experiments were conducted as shown in Fig. 1A. OVX animal models were constructed, and the indicated materials were collected. The ovaries were located through a dorsal incision (Supplementary Fig. 1A), ligated and resected. To confirm that both ovaries were completely removed from the female mice, we performed cytological and histomorphological analyses of vaginal shedding and measured the serum oestradiol levels. H&E staining of cell smears collected after vaginal irrigation revealed that the cells shed from the vagina of the mice in the Sham group were in different phases of the oestrous cycle (Supplementary Fig. 1C, a, b, c, d); specifically, in the proestrus phase, many large oval nuclear epithelial cells were detected in the visual field (Supplementary Fig. 1C, a); in the oestrous phase, many nonnucleated epithelial cells were observed in the visual field (Supplementary Fig. 1C, b); in the metestrus phase, the visual field included various cellular components, including small and round white blood cells, nonnucleated epithelial cells and large oval nucleated epithelial cells (Supplementary Fig. 1C, c); and in the dioestrus phase, the cells in the visual field were composed of a single mass of small, round white blood cells (Supplementary Fig. 1C, d). Abdominal exploration of the uterus and ovaries from the mice in the Sham group revealed that the uterus and ovaries were normal and that the uterus was thick, whereas the observations of the mice in the OVX group showed that the ovaries were completely absent without residual tissue and that the uterus was relatively small (Supplementary Fig. 1B). The serum oestradiol levels were measured by ELISA, and the results showed that the oestradiol concentration of the OVX group was significantly lower than that of the Sham group ($P < 0.001$) (Fig. 1B).

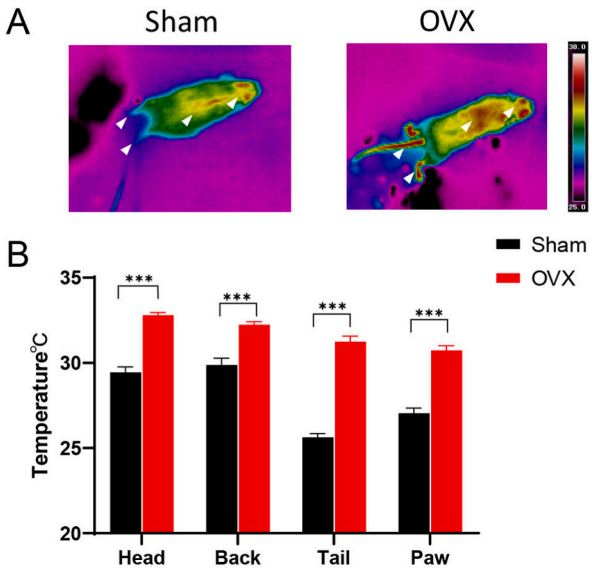

Fig. 2. Monitoring of the body surface temperature of OVX model mice. **(A)** Infrared thermographs showing the skin temperature of mice in the Sham and OVX groups. The white arrows point to the head, back, tail and paws of the mice. **(B)** Statistical analysis of the body surface temperature of the head, back, tail and paws; n = 13 biologically independent animals per group. The data are shown as the means ± SEMs, and Student's *t*-test was used to analyse the differences between the two groups; ***$P < 0.001$.

3.2. The body surface temperature was increased in OVX model mice

The body surface temperature of the mice was monitored by infrared thermography for 15 min. The average temperatures of the designated areas on the head (Sham, 29.46 ± 0.30; OVX, 32.81 ± 0.14; $P < 0.001$), back (Sham, 29.88 ± 0.4; OVX, 32.24 ± 0.17; $P < 0.001$), tail (Sham, 25.63 ± 0.21; OVX, 31.25 ± 0.31; $P < 0.001$) and paw (Sham, 27.05 ± 0.30; OVX, 30.74 ± 0.27; $P < 0.001$) were determined. Together, the results showed that the body temperature of the OVX group was greater than that of the Sham group (Fig. 2A, B).

3.3. Mapping of 5-HT, 5-HT1AR and 5-HT2AR expression in the whole brains of OVX model mice

3.3.1. Reduced number of 5-HT-positive neurons in the RN of OVX model mice

Immunohistochemical staining revealed the presence of brown 5-HT-positive puncta in the cytoplasm of RN neurons (Fig. 3A, arrows). The number of 5-HTergic neurons in the RN was significantly lower in the OVX group than in the Sham group ($P < 0.05$) (Figs. 3B and 4), and the AOD was significantly lower in the OVX group ($P < 0.05$) (Fig. 4).

3.3.2. Reduced number of 5-HT-positive nerve fibres in the brains of OVX mice

According to the fourth edition of Paxinos and Franklin's Mouse Brain in Stereotaxic Coordinates [29], we selected 10 representative coronal sections to assess the expression of 5-HTergic neurons and fibres. In brain regions other than the RN, brown 5-HT puncta were observed in the axons (nerve fibres) of 5-HTergic neurons; the puncta were either elongated and linear or dotted and linear and found widely throughout the brain. Ten representative 5-HT-positive coronal brain tissue sections (Fig. 5A–J) showing the distribution of 5-HT-positive neurons and fibres at different distances from the bregma were selected. For each group of 5 mice, the same 3 sections were selected, and the number of 5-HT-positive cells per 27,500 μm^2 was counted. In the Sham group, areas of high, medium and low 5-HT nerve fibre density were detected. High expression of 5-HT was detected in the DM, AHA, BMA, MPA and Pa; moderate expression was observed in the SCh, SPN, LH, LPO, BLA, CoA, MePV, Arc, LS, LPB, SNR, LC, DG, SNC, MnPO, CeA and MS; and low expression was detected in the CA2, CA3, CA1, cortex, cerebellum, olfactory bulb, and MPB (Fig. 5A–J). Compared with the mice in the Sham group, the mice in the OVX group showed reduced numbers of 5-HTergic fibres in 72 assayed brain regions ($P < 0.05$) (Fig. 4), lower AODs of 5-HTergic fibres in most brain regions ($P < 0.05$) (Fig. 4). Trends towards decreases in the AODs if 5-HTergic fibres in the BMA, LPB, Arc, VMH, LH, CA3, DM, and BLA ($P > 0.05$) (Fig. 4). The expression of 5-HT positive nerve fibres in the POA of the hypothalamus was predominantly observed, with a more pronounced decrease noted in the MPA compared to other brain regions, such as MnPO and LPO (Fig. 3C, D, Fig. 4). The changes in 5-HT positive nerve fibres and AOD in other brain regions are shown in Supplementary Table 1.

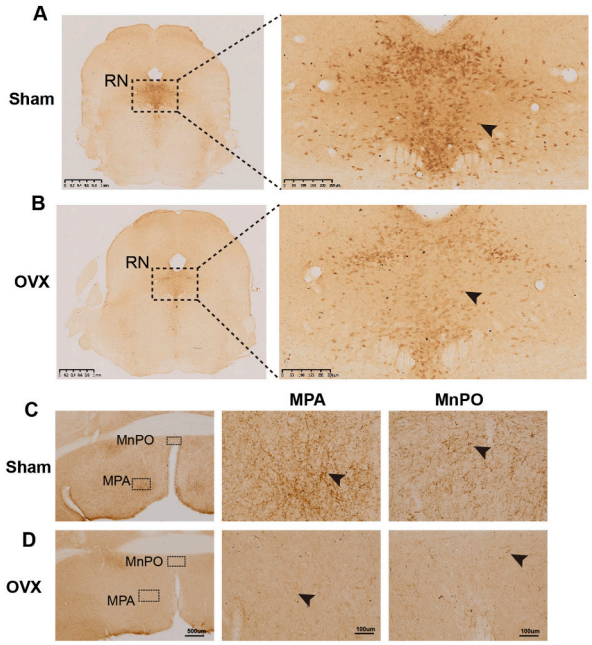

Fig. 3. Differences in the distribution of 5-HT-positive neurons in the RN and nerve fibres in the POA. **(A, B)** 5-HT-positive neurons in the Sham and OVX groups. The black arrows show the positions where apparent differences were observed. Scale bars, 1 mm and 250 μm. **(C, D)** 5-HT-positive nerve fibres of POA in the Sham and OVX groups. Scale bars, 500 μm and 100 μm.

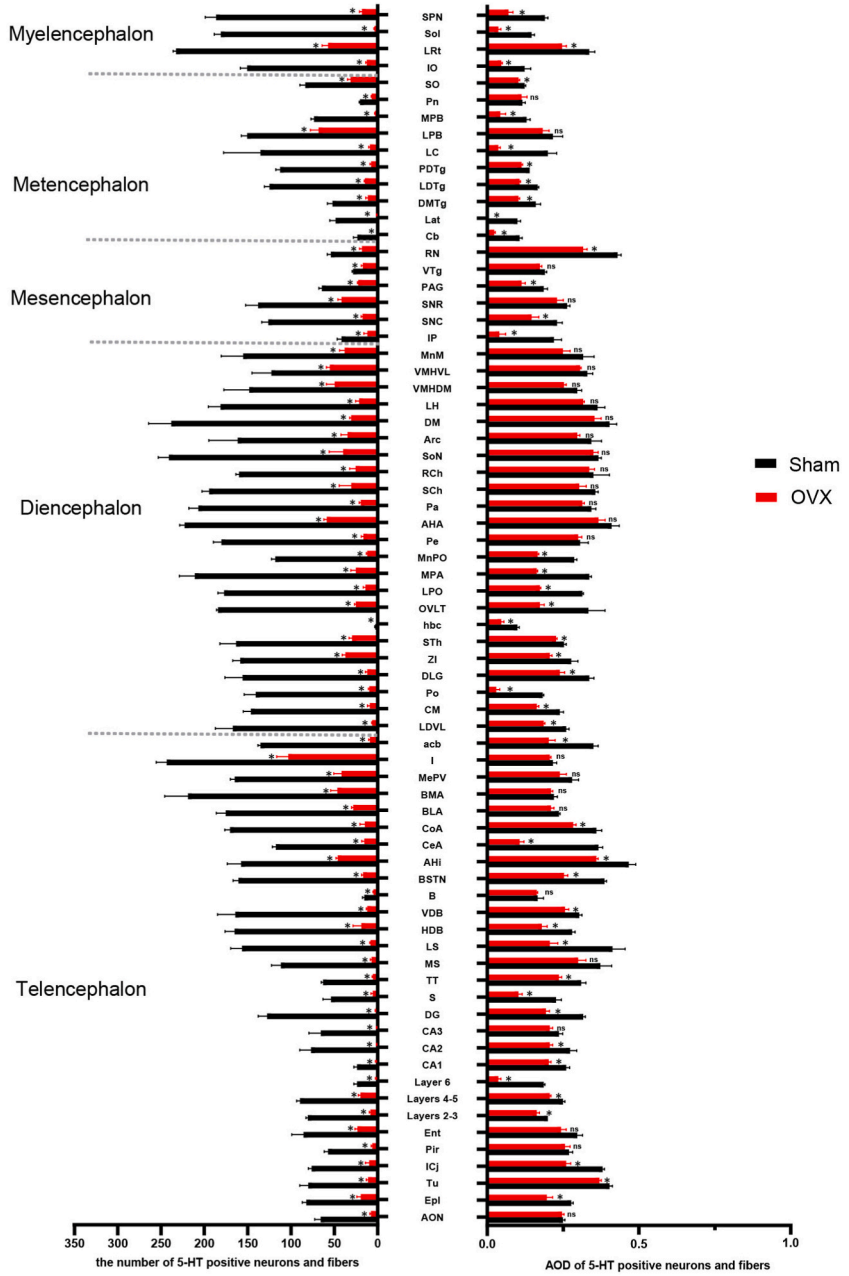

Fig. 4. Comparison of the number of 5-HT-positive neurons and fibres in the whole brain.
The numbers of positive neurons per unit area (27,500 μm^2) in different brain areas are shown. n = 3 biologically independent images per group. The data are shown as the means ± SEMs. Student's *t*-test was used to analyse the differences between the two groups; *$P < 0.05$, ns: $P > 0.05$. Source data and P values for different brain areas are shown in Supplementary Table 1. The definitions of the abbreviations for the different brain regions are provided in Table 4.

3.3.3. Distribution of 5-HT1AR and 5-HT2AR in the brains of female mice

According to the Mouse Brain Atlas as described above, we selected 10 representative coronal sections to assess the expression of 5-HT1AR and 5-HT2AR in each brain region. 5-HT1AR was widely expressed in multiple brain regions, and 5-HT2AR was expressed in some brain regions. We counted the number of 5-HT1AR- and 5-HT2AR-positive cells and detected the AOD. 5-HT1AR was expressed in the cytoplasm, cell membrane, dendrites and axons (Fig. 6A-L, arrows), and 5-HT2AR was expressed mostly in the cell membrane, dendrites and axons (Fig. 6A-L, arrows).

The number of 5-HT1AR- and 5-HT2AR-positive cells per unit area and the AODs of 5-HT1AR and 5-HT2AR in brain slices from the mice in the Sham group were determined, and the results showed that the mice in the Sham group exhibited many 5-HT1AR-positive

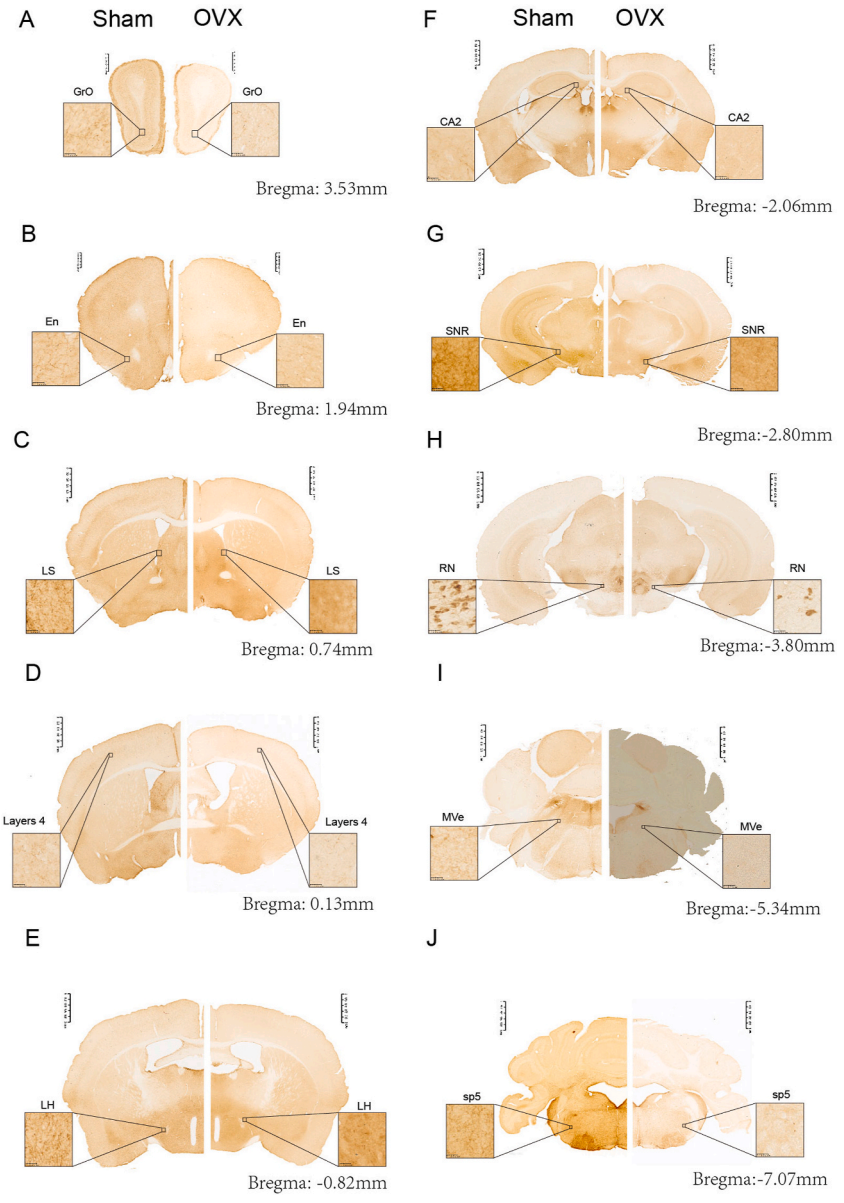

Fig. 5. Differences in the whole-brain distributions of 5-HT-positive neurons and fibres. **(A–J)** Representative coronal sections of the whole brains of mice in the Sham (left) and OVX (right) groups showing 5-HT-positive neurons and fibres. Each section has a thickness of 50 μm. Scale bar, 1 mm and 25 μm. En, endopiriform nucleus; GrO, granule cell layer of the olfactory bulb; MVe, medial vestibular nucleus; sp5, spinal trigeminal tract.

cells in the hippocampal formation (CA1, CA2, CA3, DG), tegmental area, SCh, SoN, BSTN, and AHA; a moderate number of 5-HT1AR-positive cells in the septal nucleus (LS, MS), amygdala (MePV, CeA, I, CoA, AHi), POA (MPA, MnPO), LC, PB (MPB, LPB), PAG and layers 2-5 of the cortex; and a few 5-HT1AR-positive cells in the olfactory bulb partial subnucleus, Ent, Pir, SN (SNC, SNR), Cb, LPO, BMA, BLA, and SPN. The mice in the Sham group had a moderate number of 5-HT2AR-positive cells in the SCh, RN, Cb, amygdala (MePV, CoA, BLA, BMA, CeA), LC, BSTN, SNC, MS and MnPO and few 5-HT2AR-positive cells in the hippocampal formation, POA (MPA, LPO), LH, PAG, PB (MPB, LPB), LS, SoN, Arc, AHi, I and every layer of the cortex (Fig. 6A–L, Fig. 7A1-E2, Fig. 8F1-J2, Fig. 9, Fig. 10). The changes in the expression and optical density of 5-HT1AR and 5-HT2AR are shown in Supplementary Table 1.

3.3.4. Alterations in the numbers of 5-HT1AR- and 2AR-positive neurons in different brain regions of OVX model mice

In the Sham group, 5-HT1AR was distributed across more brain regions than was 5-HT2AR. The number of 5-HT1AR-positive neurons was increased in the following brain regions: the POA (MPA, MnPO, LPO), amygdala (CoA, CeA, MePV, BLA, BMA and I), Arc, DM, PAG, LS, Pir, RN and layers 2–5 of the cortex. Decreases in the number of 5-HT1AR-positive neurons were observed in the following brain regions: Cb, hippocampal formation (CA1, CA2, CA3, DG), SPN, LC, SCh, and PB (LPB, MPB) (Fig. 6, Fig. 7A1-E2,

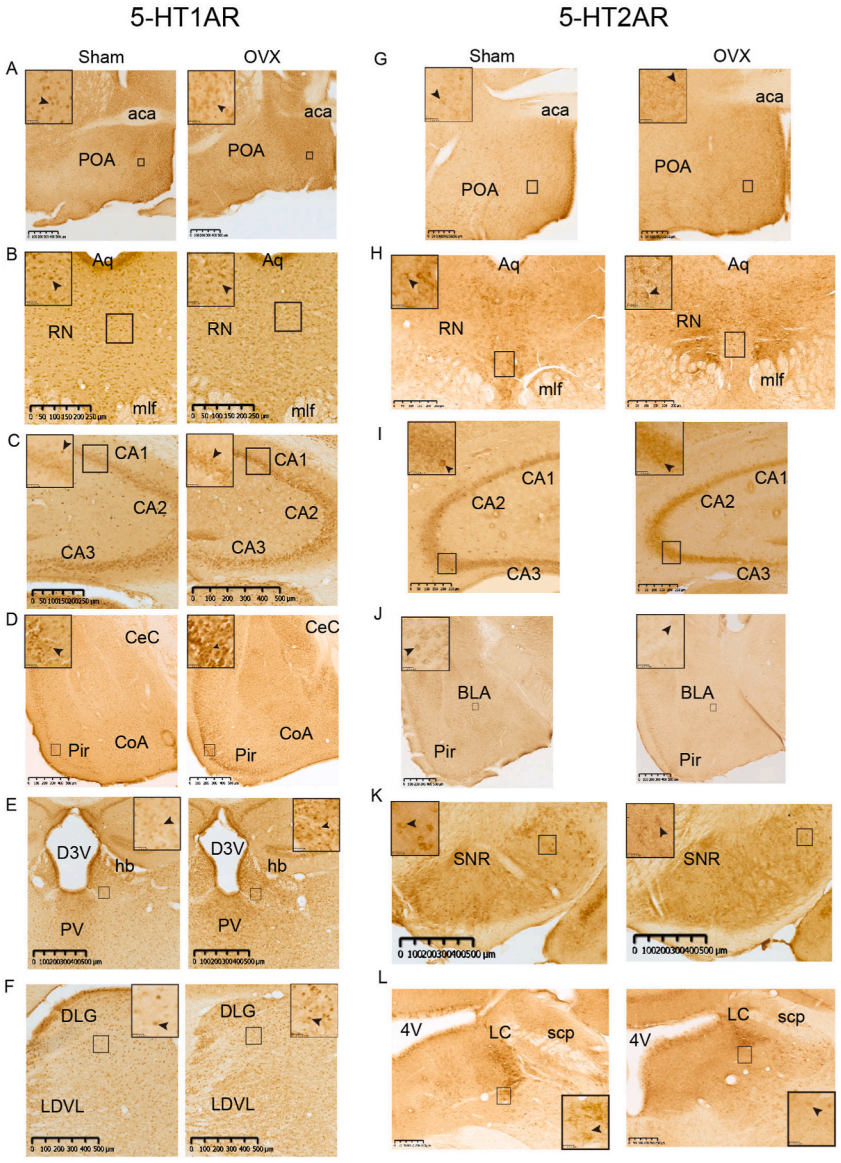

Fig. 6. Representative staining images showing the main brain regions expressing 5-HT1AR and 5-HT2AR in the Sham (left) and OVX (right) groups.
The black arrows show the positions where apparent differences were observed. Scale bar, 1 mm and 25 μm. aca, anterior commissure, anterior part; Aq, aqueduct; D3V, dorsal 3rd ventricle; hb, Habenula nucleus; mlf, medial longitudinal fasciculus; PV, paraventricular thalamic nucleus; scp, superior cerebellar peduncle; 4V, 4th ventricle.

Fig. 8F1-J2, Fig. 9, Fig. 10).

The number of 5-HT2AR-positive neurons and the optical density of 5-HT2ARs were increased in a few brain regions: POA (MPA, LPO), amygdala (BLA), every layer of the cortex, and SPN. Decreases in the number of 5-HT2AR-positive neurons were observed in most brain regions, including the RN, hippocampal formation (CA1, CA2, CA3, DG), septal nucleus (LS, MS), SNR, SNC, PB(LPB, MPB), VMH, Arc, DM, LH, AHA, PAG, SCh, LC, and Cb (Fig. 6, Fig. 7A1-E2, Fig. 8F1-J2, Fig. 9, Fig. 10). The changes in the expression and optical density of 5-HT1AR and 5-HT2AR in other brain regions are shown in Supplementary Table 1.

Here, we summarized the changes in the expression of 5-HTergic neuropathway in PMS-related brain regions (Fig. 11). We detected the following patterns: the axons of 5-Hergic neurons in the RN were distributed in all brain regions, and 5-HT1AR was detected in all fibre-expressing regions. However, there are a few brain regions with no 5-HT2AR expression.

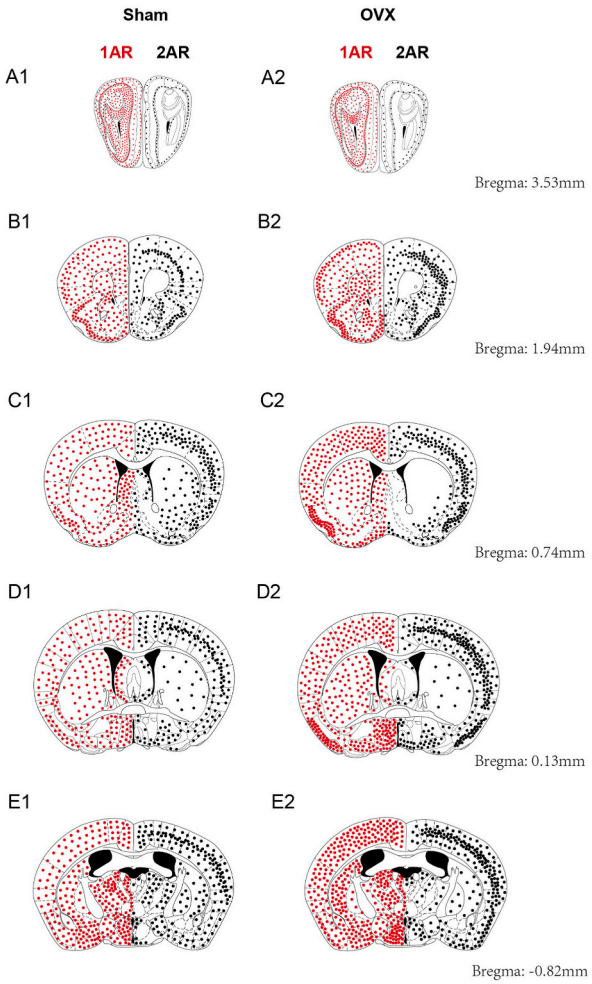

Fig. 7. Coronal brain diagrams showing the main sites of 5-HT1AR (left side, red dots) and 5-HT2AR (right side, black dots) expression in the Sham (left) and OVX (right) groups (anterior half of the brain).
The information shown in these pattern plots is simplified, and dots are used to show the number and distribution of positive cells. Small dots = 1–10 labelled cells; maps of the whole mouse brain were drawn with reference to Paxinos and Franklin's Mouse Brain in Stereotaxic Coordinates (4th Edition, 2013). (For interpretation of the references to colour in this figure legend, the reader is referred to the Web version of this article.)

3.4. Reduced ERα and ERβ expression in the RN of OVX model mice

After OVX, the levels of sex hormones, including oestrogen and progesterone, are reduced in mice, and the levels of oestrogen-related receptors in the brain may be altered [30]. Therefore, we explored the causes and mechanisms of alterations in 5-HTergic neural pathways after OVX from the perspective of oestrogen-related receptors. qPCR and WB showed that the RNA and protein expression levels of ERα and ERβ were reduced in the RN of female mice eight weeks after OVX ($P < 0.05$) (Fig. 12A, B, D, E, G, H), whereas no significant change in GPR30 expression was observed ($P > 0.05$) (Fig. 12C, F, I). Thus, ERα and ERβ may bind to genes related to 5-HT metabolism and act as transcription factors, in turn altering 5-HTergic neural pathways in the brain and triggering perimenopause-related symptoms.

3.5. ERα and ERβ act as transcription factors to regulate the expression of TPH2 and MAOA and affect the synthesis of 5-HT in the brains of female mice

To identify the 5-HT metabolism-related genes in the RN that ERα and ERβ bind to and regulate the transcription of 5-HT, middle RN tissues were collected from the mice in the Sham group, prepared as single-cell suspensions, stained with DAPI and observed under a fluorescence microscope. The nuclei were dispersed and intact (Fig. 13A), and the extracted nuclei were subjected to CUT&Tag profiling. The sequencing results showed that most of the binding sites were concentrated in the upper and lower reaches of the gene promoter about 3 kb (Fig. 13B). For ERα sequencing, 8012, 7058 and 12,241 peaks were identified in 3 replicate samples, and for ERβ sequencing, 10,727 and 9113 peaks were identified in 2 replicate samples. Manhattan plots were generated to visualize the

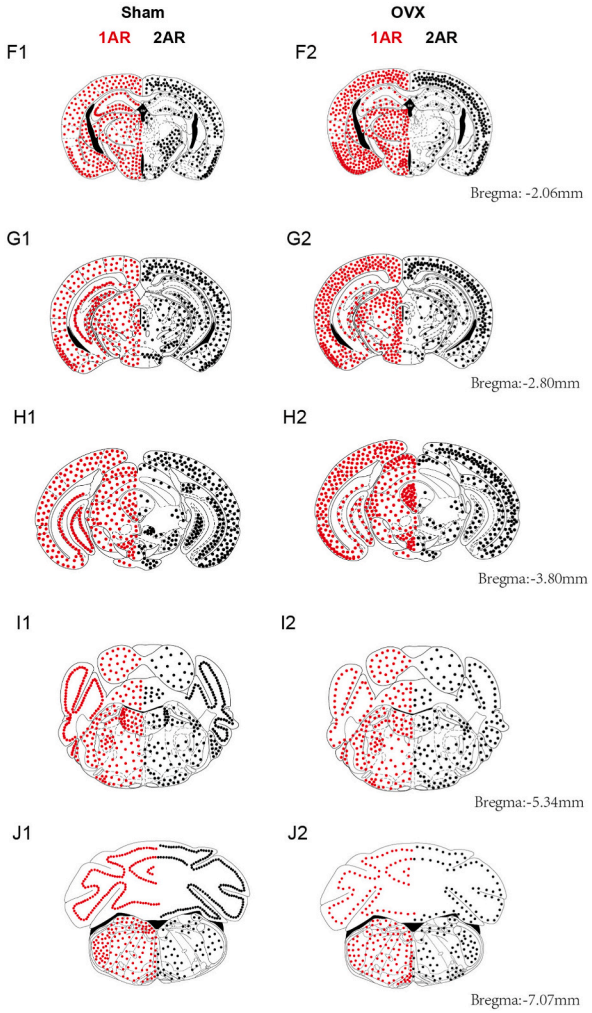

Fig. 8. Coronal brain diagrams showing the main sites of 5-HT1AR (left side, red dots) and 5-HT2AR (right side, black dots) expression in the Sham (left) and OVX (right) groups (posterior part of the brain).
The information shown in these pattern plots is simplified, and dots are used to show the number and distribution of positive cells. Small dots = 1–10 labelled cells. Maps of the whole mouse brain were drawn with reference to Paxinos and Franklin's Mouse Brain in Stereotaxic Coordinates (4th Edition, 2013). (For interpretation of the references to colour in this figure legend, the reader is referred to the Web version of this article.)

distribution of all the peaks corresponding to the two transcription factors on the mouse chromosomes (Fig. 13C, E). The experimental results were generated by concatenating the loci of the peaks identified in each replicate sample to locate the gene to which each transcription factor was bound based on the gene promoter region closest to the binding site; the peaks were classified according to their location (Fig. 13D, F). The 5-HT-bound genes, which included 5-HT-related receptors, enzymes, and transporters involved in 5-HT anabolism and transport (ERα: Fev, Tph2, Slc6a4, Maoa, Maob; ERβ: Slc6a4, Maoa) (Supplementary Table 2), were enriched in 5-HTergic neuron- and synapse-associated pathways (Fig. 14A, B).

The sequencing data were imported into SnapGene software and analysed, and the results revealed that ERα regulates the transcription of TPH2. CUT&Tag profiling was used to screen two loci located at the promoter of the TPH2 gene, i.e., 115186476–115186974 and 115185960–115186458 on chromosome 10 (Fig. 15A, B). ERα was also found to regulate the transcription of MAOA, and two loci were found in the promoter sequence of the MAOA gene, 16617703–16618201 and 16617939–16618437, on chromosome X (Fig. 15C, D). ERβ was found to regulate the transcription of MAOA, and two loci were found in the promoter sequence of the MAOA gene, 16618034–16618532 and 16618046–16618544, on chromosome X (Fig. 15E, F). The detailed sequences of the abovementioned loci are shown in Supplementary Table 3, and the positions of the loci are shaded grey with IGV software. A dual-luciferase gene reporter assay was performed to verify that ERα and ERβ regulate the transcription of these target genes, and the findings showed that both ERα and ERβ positively regulate the transcription of the TPH2 and MAOA genes (Fig. 15B, D, F). Maps of the motifs of the transcription factors that acted on the promoters of the genes were drawn based on the obtained sequences, imported into https://meme-suite.org/meme/, and analysed with MEME Suite 5.5.0; compared with the structure maps on the JASPAR website (Fig. 15J, K); and compared to the map of the motif predicted by the website (Fig. 15G, H, I). The similarity of the

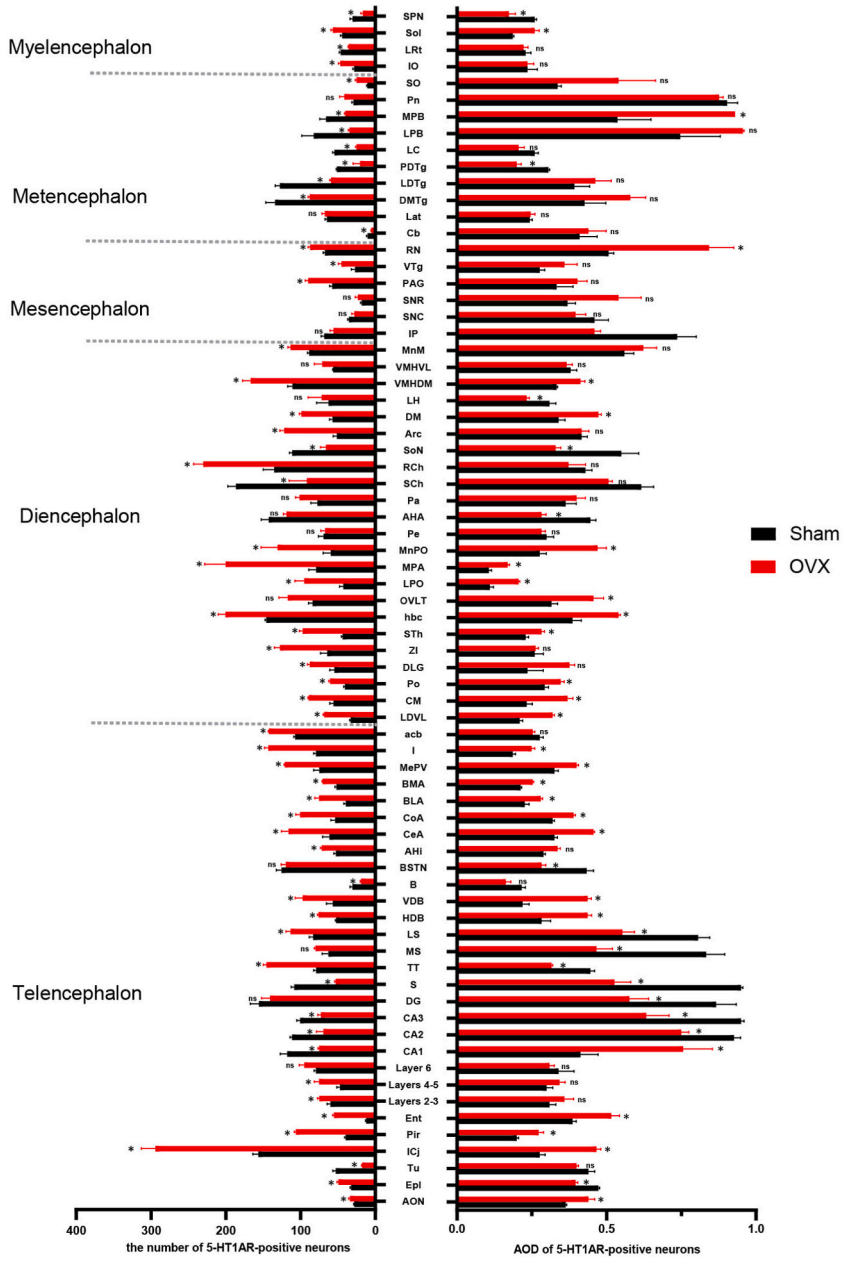

Fig. 9. Comparison of the number and AOD of 5-HT1AR-positive neurons in the whole brain.
The numbers of positive neurons per unit area (27,500 μm^2) in different brain areas are shown; n = 3 biologically independent images per group. The data are shown as the means ± SEMs. Student's *t*-test was used to analyse the differences between the two groups; *$P < 0.05$, ns: $P > 0.05$. Source data and P values for different brain areas are shown in Supplement Table 1. The definitions of the abbreviations used for different brain regions are provided in Table 4.

map to that of the predicted motif on the website showed that the results were credible.

3.6. ERs regulate the RNA and protein levels of TPH2 and MAOA and affect the mouse body temperature through the 5-HTergic neural pathway

The CUT&Tag results were imported into SnapGene, and the analysis revealed that the transcription factor ERα has binding sites in the promoter regions of TPH2 and MAOA and that the transcription factor ERβ has binding sites in the promoter region of MAOA. To verify that ERα and ERβ regulate the transcription of TPH2 and MAOA, we performed mechanistic studies in vivo and in vitro and assessed the effects of ERα and ERβ on the body temperature of the mice.

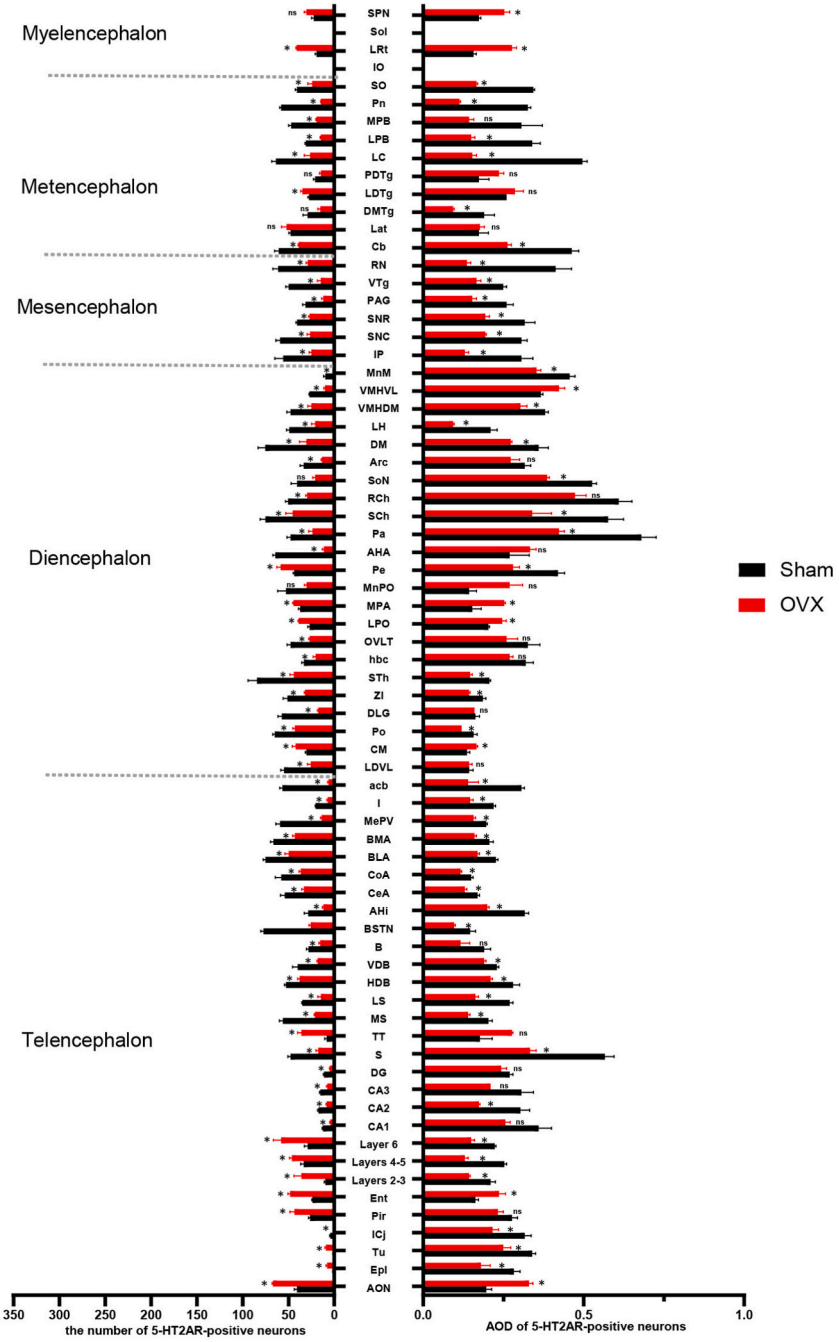

Fig. 10. Comparison of the number and AOD of 5-HT2AR-positive neurons and fibres in the whole brain.
The numbers of positive neurons per unit area (27,500 μm^2) in different brain areas are shown; n = 3 biologically independent images per group. The data are shown as the means ± SEMs. Student's *t*-test was used to analyse the differences between the two groups; *$P < 0.05$, ns: $P > 0.05$. Source data and P values for different brain areas are shown in Supplement Table 1. The definitions of the abbreviations used for different brain regions are provided in Table 4.

The results of a dual-luciferase gene reporter assay showed that ERα positively regulates the transcription of TPH2 and MAOA and that ERβ positively regulates the transcription of MAOA (Fig. 15B, D, F).

To investigate the effects of ERα and ERβ on the 5-HT levels in the RN and body temperature and the underlying mechanisms, we injected ERα and ERβ activators into the RN of the mice in the Sham group and ERα activators and ERβ activators into the RN of the mice in the OVX group. Then we measured the 5-HT content, the RNA and protein expression level of TPH2 and MAOA in the mouse RN.

		5-HT		5-HT1A receptor		5-HT2A receptor	
brain structure	brain region	numbers	AOD	numbers	AOD	numbers	AOD
cortex	Pir	↓	ns	↑	↑	↑	ns
	Ent	↓	ns	↑	↑	↑	↑
	Layers 2-3	↓	↓	↑	ns	↑	↓
	Layers 4-5	↓	↓	↑	ns	↑	↓
	Layer 6	↓	↓	ns	ns	↑	↓
preoptic area(POA)	MPA	↓	↓	↑	↑	↑	↑
	MnPO	↓	↓	↑	↑	ns	ns
	LPO	↓	↓	↑	↑	↑	↑
arcuate nucleus	Arc	↓	ns	↑	ns	↓	ns
dorsomedial nucleus	DM	↓	ns	↑	↑	↓	↓
lateral hypothalamus	LH	↓	ns	ns	↑	↓	↓
nucleus accumbens	acb	↓	↓	↑	ns	↓	↓
amygdaloid nucleus	AHi	↓	↓	ns	ns	↓	↓
	CeA	↓	↓	ns	↑	↓	↓
	CoA	↓	↓	↑	↑	↓	↓
	BLA	↓	ns	↑	ns	↓	↓
	BMA	↓	ns	↑	↑	↓	↓
	MePV	↓	ns	↑	ns	↓	↓
	I	↓	ns	↑	↑	↓	↓
hippocampus	CA1	↓	↓	↓	↑	↓	ns
	CA2	↓	↓	↓	↓	↓	↓
	CA3	↓	ns	↓	↓	↓	ns
	DG	↓	↓	ns	↓	↓	ns
periaqueductal gray	PAG	↓	↓	↑	ns	↓	↓
raphe nucleus	RN	↓	↓	↑	↑	↓	↓
cerebellum	Cb	↓	↓	↓	ns	↓	↓
locus ceruleus	LC	↓	↓	↓	ns	↓	↓
substantia nigra	SN	↓	ns	ns	ns	↓	↓
suprachiasmatic nucleus	SCh	↓	ns	↓	ns	↓	↓

Fig. 11. Corresponding relationships between changes in 5-HTergic neural pathways in key brain regions.
↑, increased expression in the OVX group. ↓, decreased expression in the OVX group. ns, no sense

The RNA and protein levels of MAOA were lower in the brains of the OVX model mice than in those of the Sham mice ($P < 0.05$) (Fig. 16B, D, H), and the RNA and protein levels of TPH2 were lower in the brains of the mice in the OVX group than in those of the mice in the Sham group ($P < 0.01$) (Fig. 16C, E, G). The skin surface temperature of the mice in the OVX group was higher than that of the mice in the Sham group ($P < 0.05$) (Fig. 16F, I).

The 5-HT content in the RN was lower in the mice in the Sham group after injection of an ERα depressor and an ERβ depressor into the RN than in those of the mice in the Sham group that were not injected ($P < 0.05$) (Fig. 16A); moreover, the RNA and protein levels of TPH2 were lower in the brains of the mice in the drug-treated Sham group than in those of the mice in the untreated Sham group ($P < 0.01$) (Fig. 16C, E, G), and the RNA and protein levels of MAOA were lower in the brains of the mice in the drug-treated Sham group than in those of the mice in the untreated Sham group ($P < 0.0001$) (Fig. 16B, D, E, H). The body surface temperature in back, tail, and paw temperatures of the mice in the drug-treated Sham group were lower than those of the mice in the untreated Sham group ($P < 0.05$) (Fig. 16F, I).

The 5-HT concentration was greater in the mice in the OVX group after injection of an ERα activator or an ERβ activator into the RN than in the OVX model mice ($P < 0.001$) (Fig. 16A); moreover, the RNA and protein levels of TPH2 were greater in the brains of the mice in the drug-treated OVX group than in those of the mice in the untreated OVX group ($P < 0.05$) (Fig. 16C, E, G), and the RNA and protein levels of MAOA were greater in the brains of the mice in the drug-treated OVX group than in those of the mice in the untreated OVX group ($P < 0.05$) (Fig. 16B, D, E, H). The body surface temperature in back, tail, and paw temperatures of the mice in the drug-treated OVX group were lower than those of the mice than in the untreated OVX group ($P < 0.001$) (Fig. 16F, I).

4. Discussion

The development of PMS is associated with alterations in 5-HTergic neural pathways in the brain. Therefore, elucidating the changes in 5-HTergic neural pathways that occur in the brain after OVX is important for obtaining a better understanding of the pathology of PMS. In this study, we provide information on the whole-brain distribution of 5-HT and its receptors (5-HT1AR and 5-HT2AR) in the mouse brain after OVX. Prolonged periods of low oestrogen levels during perimenopause result in changes in ER expression. The current study revealed that the expression of ERα and ERβ in the RN was significantly reduced after OVX and that ERα and ERβ positively regulate the transcription and translation of TPH2 and MAOA, resulting in perimenopause-related symptoms (e.g., changes in body temperature) (Fig. 16F, I); thus, TPH2 and MAOA may be new targets for the diagnosis and treatment of perimenopause-related symptoms. Fig. 17 shows a diagram of the whole study.

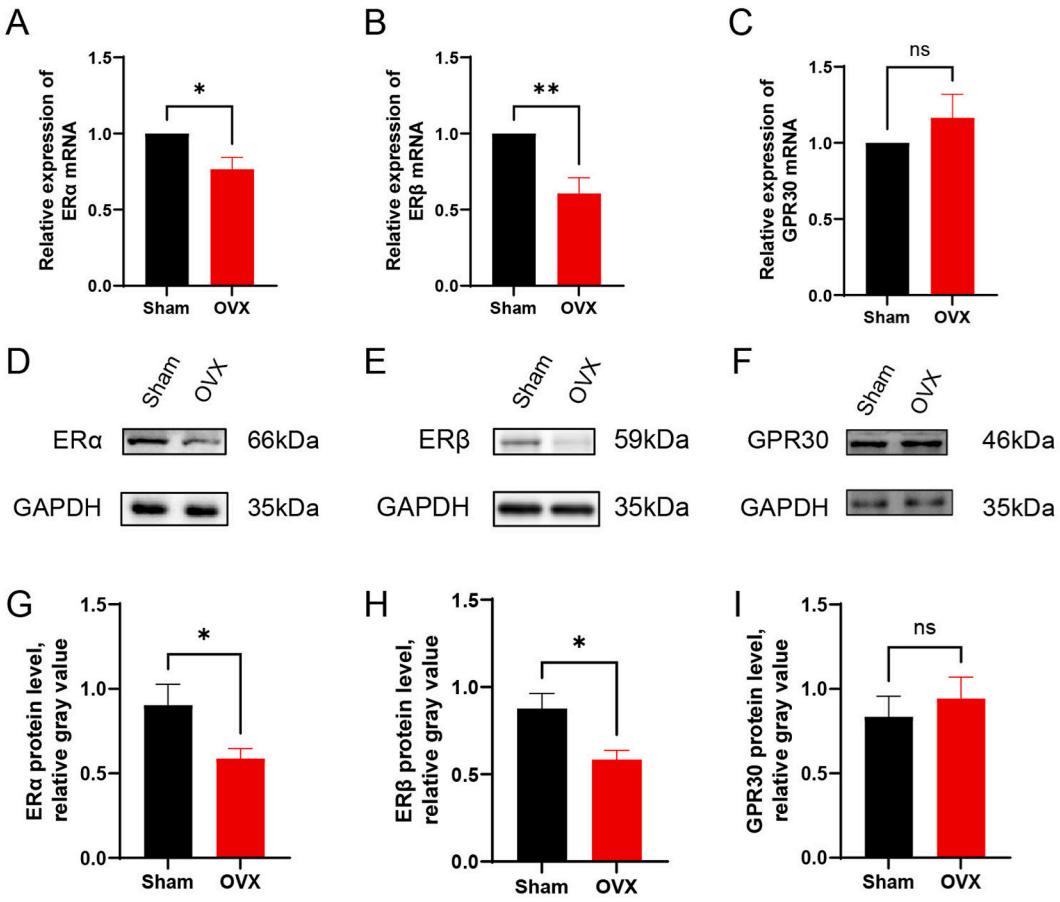

Fig. 12. Comparison of the expression of ERα, ERβ and GPR30 in the RN. **(A-C)** Relative mRNA levels of ERα, ERβ and GPR30. **(D–F)** Representative immunoblots of ERα, ERβ and GPR30. See Supplementary Material 1 for the original image that has not been cropped. **(G-I)** Relative protein levels of ERα, ERβ and GPR30; n = 5 biologically independent animals per group. The data are shown as the means ± SEMs. Student's *t*-test was used to analyse the differences between the two groups; $^{*}P < 0.05$, $^{**}P < 0.01$; ns: $P > 0.05$.

Part 1. Mapping of 5-HT, 5-HT1AR and 5-HT2AR expression in the whole brains of OVX model mice.

The specific roles and effects of 5-HT and its receptors in various brain regions related to the body temperature, mood, sleep, learning and memory have been extensively studied in male mice via in situ mRNA hybridization, and these data are available at http://portal.brain-map.org/. The present study was performed to systematically explore the role of 5-HT and its receptors in PMS by assessing the expression of these molecules in female mice before and after OVX. In the brain regions that are responsible for relevant physiological functions (body temperature, mood, sleep, learning and memory), 5-HT plays a role in hot flashes, depression, insomnia and AD.

Among all 5-HT-related receptors, 5-HT1AR, which is regarded as a presynaptic receptor, is the only subtype expressed on 5-HTergic neurons [31]. In addition, both 5-HT1AR and 2AR are expressed on postsynaptic cells and mediate the hyperpolarization and depolarization of neurons [32]. Therefore, these two genes may regulate opposite physiological functions in the same brain to maintain physiological stability [33]. The expression of these two genes in the same brain area is a valuable topic for further study and discussion.

The thermoregulatory centre is located in the preoptic area, and the alterations in 5-HT-positive nerve fibres in the hypothalamic preoptic areas of mice after OVX were analysed. The number of 5-HT-positive fibres in multiple subnuclei (MnPO, MPA, and LPO) within the preoptic area was generally reduced in the OVX group compared with the Sham group, and the most pronounced reduction was observed in MPA (Fig. 3C, D). In contrast, Wenjuan Wang reported that the reduction in 5-HT-positive nerve fibres was most pronounced in vLPO in OVX rats [8]. The inconsistencies may be related to differences in the species of the experimental animals. After OVX, the expression of both 5-HT1AR and 5-HT2AR was increased in the thermoregulatory centre (Fig. 6A–G), but the content of 5-HT, which acts as a ligand for these receptors, was decreased, rendering 5-HT1AR and 5-HT2AR dysfunctional; these changes eventually manifest as a functional imbalance between heat production and dissipation and a higher body surface temperature [7]. Moreover, elevations in the temperature setpoint and metabolism also lead to an increase in the body surface temperature of OVX mice. The temperature setpoint is a hypothesis for explaining animal body temperature changes and includes the thermal and cold thresholds of

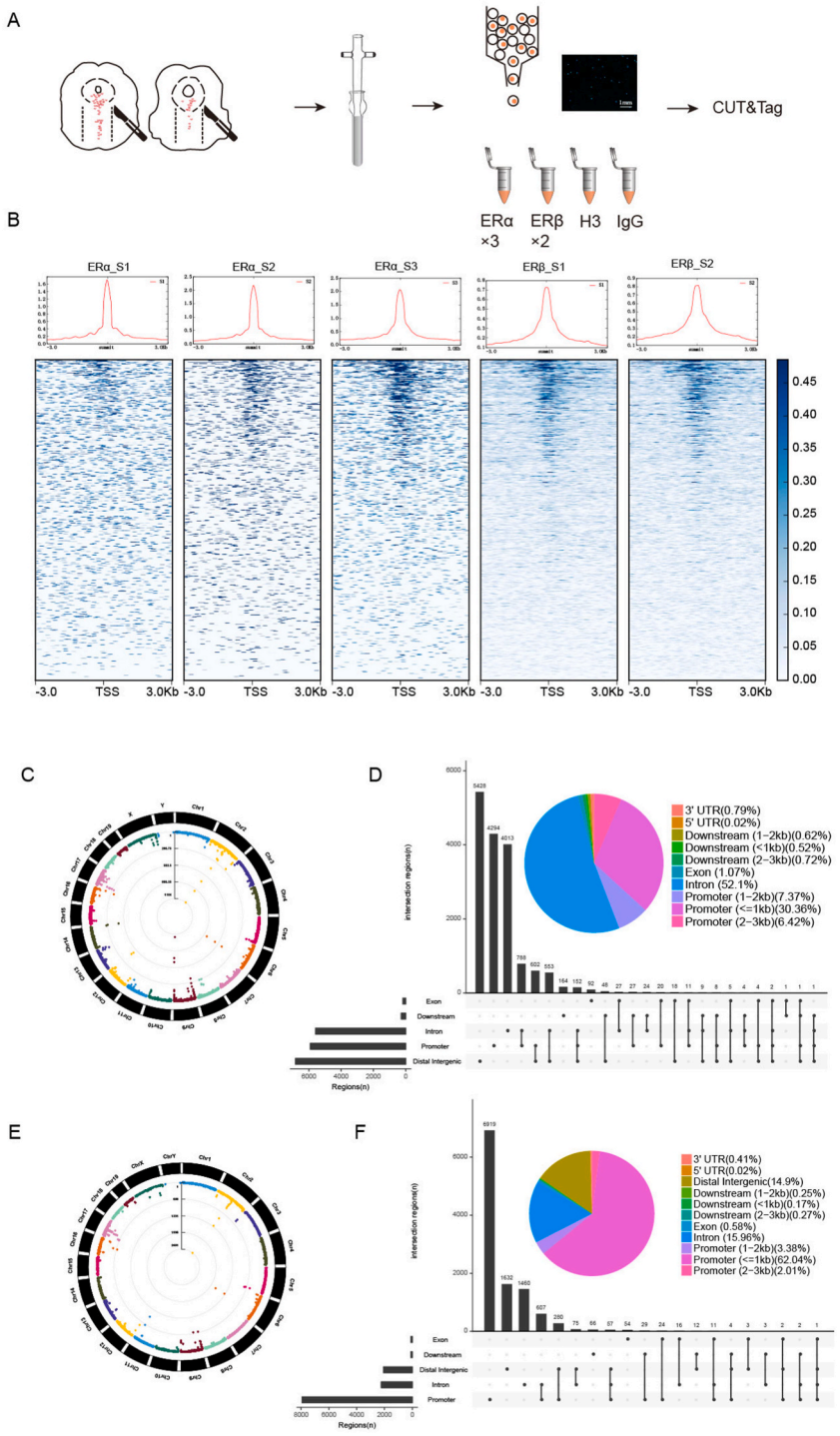

Fig. 13. CUT&Tag profiling of oestrogen nuclear receptors as transcription factors in the RN. **(A)** Schematic representation of the CUT&Tag experiments. Single-nucleus suspensions were prepared from the RN (n = 15 brains) and examined by microscopy after DAPI staining. Scale bar, 1 mm. (B**)** Line graphs and heatmaps showing the average signal distribution across the 3kb region upstream and downstream of the TSS for each sample. The images are representative of 3 (ERα) and 2 (ERβ) biological replicates. **(C, E)** Manhattan plot of the genome peaks of ERα (C) and ERβ (E) obtained by CUT&Tag profiling. The results were obtained from 3 (ERα) and 2 (ERβ) RN samples. Each dot in the circle represents a genomic DNA fragment bound by ERα (C) or ERβ (E), and the location of the dot indicates the position of the fragment within the corresponding chromosome. **(D, F)** Pie charts showing the distribution characteristics of peaks in the genome for ERα (D) and ERβ (F). The bars represent the overlapping annotation distribution of peaks in the genome. The data were pooled from 3 (ERα) and 2 (ERβ) biological replicates.

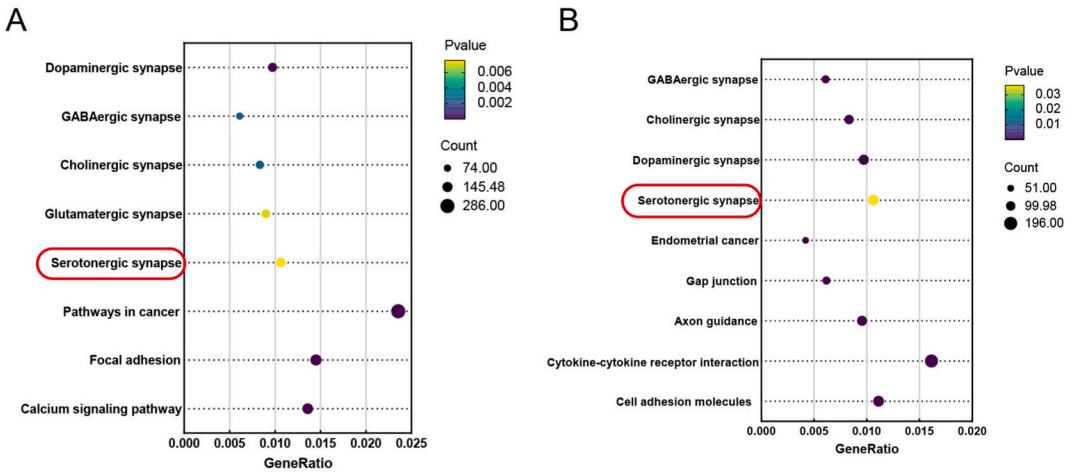

Fig. 14. KEGG pathway analysis of the genome peaks identified by CUT&Tag profiling. **(A)** Bubble diagram of the genome peaks of ERα. The red box highlights the 5-HTergic neural pathway, which was the focus of this study. **(B)** Bubble diagram of the genome peaks of ERβ. (For interpretation of the references to colour in this figure legend, the reader is referred to the Web version of this article.)

the thermal neutral zone (located in the POA). Heat- and cold-sensitive neurons located in the POA regulate these two thresholds. 5-HT1AR and 5-HT2AR are distributed on heat- and cold-sensitive neurons, respectively, and regulate the heat dissipation and heat production of neurons to maintain the body temperature within the normal temperature setpoint range. After OVX, a decrease in the 5-HT transmitter increases the expression of 5-HT1AR and 5-HT2AR in the POA, which changes the function of heat- and cold-sensitive neurons and narrows the thermal neutral zone (decreasing the thermal threshold and increasing the cold threshold). An increase in the cold threshold led to an increase in the firing frequency of cold-sensitive neurons, and an increase in the heat production response (activated nonshivering and shivering thermogenesis, vasoconstriction, and inhibited water evaporation) resulted in an increase in the surface temperature of ovariectomized mice. After the thermal threshold decreases, small temperature fluctuations in the external environment can cause the body temperature to exceed the thermal threshold, trigger the heat dissipation response of heat-sensitive neurons, and increase the likelihood of hot flashes (vasodilation) and other heat dissipation responses (sweating, inhibited nonshivering and shivering thermogenesis). Eventually, increases in temperature and metabolism lead to an imbalance between heat production and dissipation. As a result, relatively more heat is produced, resulting in an increase in the body surface temperature.

The brain regions related to emotion regulation include the RN, amygdala, frontal cortex, and hippocampus. After OVX, the number of 5-HT1AR-positive neurons in the cortex, amygdala and RN increased (Fig. 11). Michel Cyr examined the changes in the mRNA levels of 5-HT2AR in OVX model rats and reported that the mRNA levels were decreased in the CoA and anterior frontal cortex [34], consistent with the trend observed in the present study (Fig. 11).

Studies have shown sex differences in the specific manifestations of depression because men exhibit increased levels of anger, irritability and symptomatic substance intake, whereas women tend to exhibit increased sleepiness, distance from friends and heaviness in the extremities [35]. Thus, we speculate that oestrogen may play an important role in this phenomenon. Jing Ren reported that different 5-HTergic neural pathways in the brain have opposite effects in response to punishment; amygdala-projecting serotoninergic neurons in the RN promote anxiety-like behaviour, whereas frontal cortex-projecting neurons promote active coping in the face of challenge [36]. Accordingly, we focused more on the changes in 5-HT1AR and 5-HT2AR expression in the amygdala, which may be strongly related to the occurrence of depression in perimenopausal women (anxiety-like behaviour). We divided the amygdala into seven major regions: AHi, CeA, CoA, BLA, BMA, MePV and I [37]. In OVX model mice, the number of 5-HT1AR-positive neurons was increased in the CoA, BLA, BMA, MePV and I, and the AOD of 5-HT1AR was increased in the CeA, CoA and BMA (Fig. 6D). However, the number and AOD of 5-HT2AR-positive neurons were decreased in the AHi, CeA, CoA, BLA, BMA, MePV and I (Fig. 6J). Consequently, 5-HT1AR and 5-HT2AR in the amygdala may contribute to the development of perimenopausal depression. Ya Wang reported that the coadministration of 5-HT1AR and a 5-HT2AR agonist relieved anxiety-like behaviours in perimenopause [37].

The hippocampus is associated with depression [39], and we found that the expression levels of both 5-HT1AR and 5-HT2AR in the CA1, CA2, CA3 and DG were reduced in the OVX group. Antagonizing 5-HT1AR in the hippocampus can lead to anxiety by decreasing the synapse density, spine density, dendrite complexity, neurogenesis and synapsin and spinophilin expression. However, the transcription factor cAMP response element-binding protein (CREB), which is involved in hippocampal functions, can reverse this process [40]. Learning and memory impairments, the main manifestations of 'AD, are associated with the β-amyloid (Aβ) protein in the hippocampal formation. Inhibition of 5-HT1AR can decrease the levels of neuroinflammation factors and Aβ through the NF-κB signaling pathway [41]. We found that in the CA1 region, the number of 5-HT1AR-positive neurons was decreased. Studies have shown that impaired 5-HT1AR contributes to hyperactivity of pyramidal neurons (PNs) in CA1, which is an early event in AD. Activation of the RN-CA1 neuropathway can improve memory in AD model mice, and this effect is mediated by 5-HT1AR [42]. Therefore, we found that changes in 5-HT1AR and 2AR in the hippocampus may be the basis of learning and memory changes in perimenopausal mice. We found that 5-HT1AR was mainly distributed in the pyramidal cell layer (Py) and that 5-HT2AR was mainly distributed in the radial

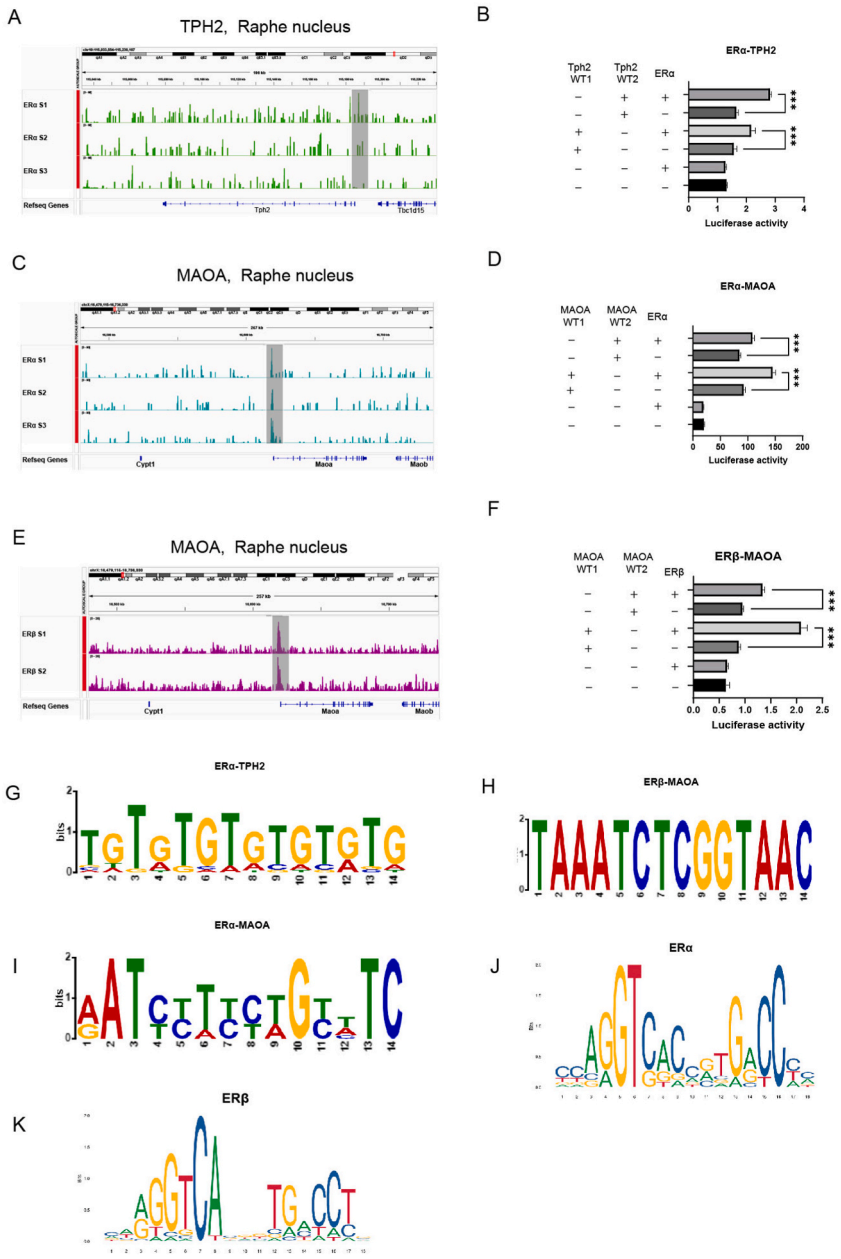

Fig. 15. CUT&Tag profiling of oestrogen nuclear receptors as transcription factors in the RN.
(A, C, E) Integrative Genome Viewer plots showing the peak distribution of CUT&Tag signals (ERα and ERβ) at TPH2 (A) and MAOA (C, E). The promoter region of the gene is shaded in grey. The data are representative of three (A, C) or two (E) independent experiments.
(B, D, F) The transcription of ERα at TPH2 (B) and MAOA (D) and that of ERβ (F) at MAOA revealed two sites in the promoter region. CUT&Tag profiling of ERα and ERβ was performed in SY5Y cells via a dual-luciferase assay. The y-axis represents luciferase activity. The data are shown as the means ± SEMs; n = 3 biologically independent experiments per group. Student's *t*-test was used to analyse the differences between the two groups; $^{***}P < 0.001$.
(G, H, I) Logo representation of the motif found by CUT&Tag profiling of ERα (G and I) and ERβ (H) and its alignment with the motif of the transcription factors ERα and ERβ retrieved from the Jaspar database.
(J, K) Examples of the top known motifs of ERα (J) and ERβ (K) obtained from https://jaspar.genereg.net/.

body layer (Rad). 5-HT1AR and 5-HT2AR expression in the hippocampal formation was decreased (Fig. 6C, I).

In the cortex, 5-HT1AR was evenly distributed in layers 2–6, and 5-HT2AR was more concentrated in layers 4–5. Research has shown that 5-HT2AR-positive neurons in layer 5 mediate the release of glutamate from pyramidal neurons, and these cortical projections modify the activity of subcortical brain regions such as the hippocampus and amygdala [43]. After OVX, 5-HT1AR expression

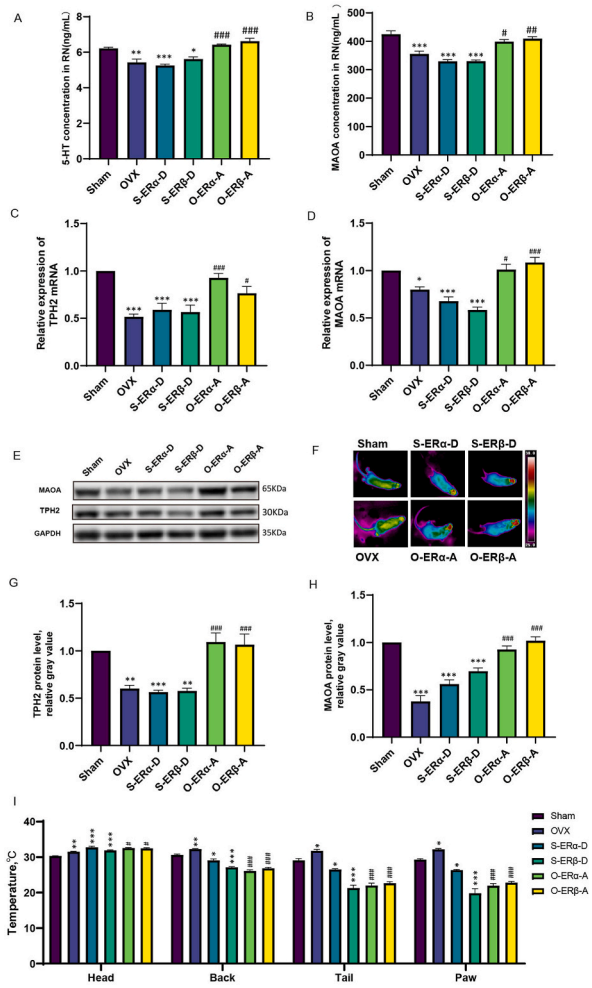

Fig. 16. Effects of the transcription factors ERα and ERβ on the transcription and translation of MAOA and TPH2 in the RN. **(A, B)** 5-HT and MAOA concentrations in the RN. S-ERα-D, Sham mice injected with an ERα depressor; S-ERβ-D, Sham mice injected with an ERβ depressor; O-ERα-A, OVX mice injected with an ERα activator; O-ERβ-A, OVX mice injected with an ERβ activator. **(C, D)** Relative mRNA levels of TPH2 and MAOA. **(E)** Representative immunoblots of MAOA and TPH2. See Supplementary Material 2 for the original image that has not been cropped. **(F)** Infrared thermographs showing the mouse skin temperature. **(G, H)** Relative protein levels of MAOA and TPH2. **(I)** Statistical analysis of the body surface temperature of the head, back, tail and paws. The data in A-D and G-I are shown as the means ± SEMs; n = 5 biologically independent animals per group. The data were analysed by one-way ANOVA followed by Tukey's multiple comparisons test. $*P < 0.05$, $**P < 0.01$, and $***P < 0.001$ compared with the Sham group. $\#P < 0.05$, $\#\#P < 0.01$, and $\#\#\#P < 0.001$ compared with the OVX group.

was increased in most layers, the number of 5-HT2AR-positive neurons was increased in the cortex, and the AOD of 5-HT2AR was decreased, which may be related to the decrease in 5-HT2AR distributed in the axons of nerve cells after OVX.

Multiple brain areas are involved in the maintenance of sleep and wakefulness. The brain regions that regulate sleep are the SCh, RN, LC, POA and reticular structures. The expression of both 5-HT1AR and 5-HT2AR was decreased in the SCh and LC but increased in the RN and POA. A study showed that 5-HT1AR in the RN and reticular formation is involved in rapid eye movement (REM) sleep [44, 45], and both 5-HT1AR and 5-HT2AR are essential for general anaesthesia awakening [46]. The hypothalamic preoptic area is associated with thermoregulation and sleep [47].

In summary, 5-HT-positive nerve fibres and 5-HT1AR are widely distributed in the brain, 5-HT-positive neurons are concentrated in the RN, and 5-HT2AR is not widely distributed in the brain. In most brain regions, 5-HT1AR and 5-HT2AR are expressed on 5-HT-positive nerve fibres; however, the cerebellum and hbc has few 5-HT-positive nerve fibres and exhibits high expression of 5-HT1AR and 5-HT2AR.

Part 2. ERα and ERβ act as transcription factors to regulate the expression of TPH2 and MAOA and affect the synthesis of 5-HT in the brains of female mice

The distribution of 5-HT-positive nerve fibres and their receptors in various brain regions is associated with changes in 5-HTergic neurons in the brain. Our previous study showed that after OVX, the number of 5-HT-positive neurons in the RN of rats decreased, but

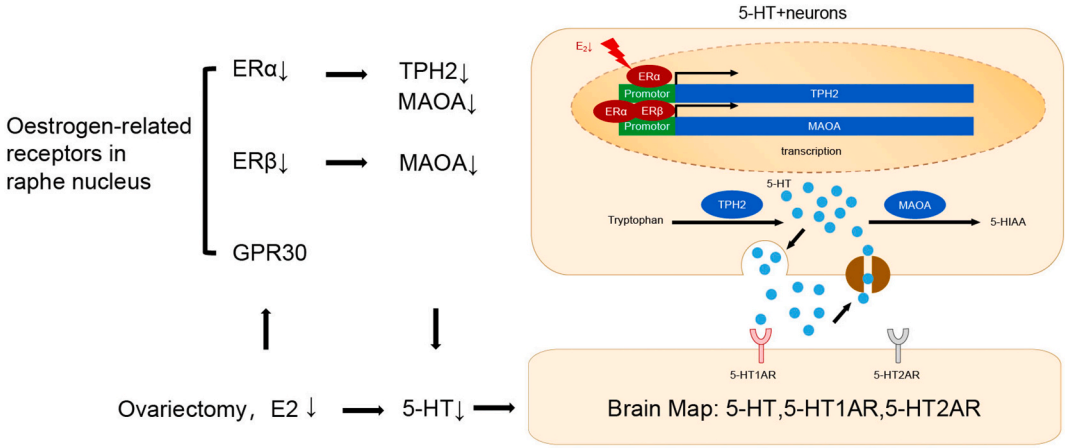

Fig. 17. Schematic representation of the changes in the 5-HTergic neural pathways in mice after ovariectomy and the underlying mechanisms. 5-HT, 5-hydroxytryptamine; 5-HTIAA, 5-hydroxyindole acetic acid; 5-HT1AR, 5-HT1A receptor; 5-HT2AR, 5-HT2A receptor; E2, oestradiol; ERα, oestrogen receptor α; ERβ, oestrogen receptor β; GPR30, G-protein coupled receptor 30; TPH2, tryptophan hydroxylase; MAOA, monoamine oxidase A.

neuronal apoptosis did not occur. However, the decrease in the number of 5-HTergic neurons was caused by a decrease in the intraneuronal 5-HT concentration [8]. Donner, N., reported that the expression of TPH2, a key enzyme for 5-HT synthesis in the RN, decreased after OVX and that TPH2 expression in the RN of OVX rats increased in response to local or systemic application of ERβ agonists [24]. Hiroi, R. studied the mechanism underlying this phenomenon and reported that ERβ regulates the expression of human TPH2 by binding to an oestrogen response element in the 5′ untranslated region, revealing the molecular mechanism by which ERβ affects the transcription of TPH2 [25]. ERβ is a key factor affecting the level of 5-HT. Both ERα and ERβ are expressed on 5-HT-positive neurons in the mouse brain [48], but the effect of ERα on molecules related to 5-HT metabolism remains unclear. In the present study, we found that ERα and ERβ expression in the RN was reduced during a prolonged hypoestrogenic state (eight weeks after OVX). This finding is consistent with the trends found for ERα and ERβ expression in the hippocampus [30], LC [49], and POA [50] after OVX, and the same trends have been observed in the ageing human brain [23]. Studies on the mechanisms of action of ERα and ERβ on 5-HT metabolism-related enzymes have been limited to the relationship between ERβ and TPH2, but we revealed that ERα also acts on the mouse TPH2 promoter to regulate TPH2 transcription. We analysed whether the expression of other metabolism-related molecules, such as MAOA, is affected by ERα and ERβ, and found that both ERα and ERβ acted on sites in the MAOA promoter. Both ERα and ERβ positively regulate MAOA expression. Therefore, we revealed the regulatory mechanism of the oestrogen receptor and 5-HT metabolism-related molecule transcription. After ovary removal, the expression of ERα and ERβ in the RN decreased, and the decreases in these transcription factors decreased the expression levels of the positive regulator of the synthetase TPH2 and the degrading enzyme MAOA, resulting in a decrease in the 5-HT content. We suspect that the content of 5-HT is determined by the relative levels of TPH2 and MAOA because 5-HT is the outcome of the relative activities of the enzymes. A reduced TPH2 concentration reduces the synthesis of 5-HT; thus, even a reduced expression of MAOA is not sufficient to increase the content of 5-HT by reducing its degradation. Ovary removal has a more obvious effect on synthetase activity, a reduction in the activity of the synthetase has a greater impact on the 5-HT content, and a reduction in the level of the degrading enzyme MAOA is not sufficient to increase 5-HT content. The synergistic effect of both factors and their equilibrium necessitate further investigation in subsequent stages. Similarly, our previous research revealed that the expression of DβH, a key enzyme for NE synthesis, and MAOA, a degradation enzyme, was reduced in rats after OVX [49].

ERα and ERβ may act as transcription factors to regulate the transcription and translation of many target genes. Based on our screening of their target genes, we found that ERα also binds to the promoter of PET1 (data not shown). PET1 is an important transcription factor associated with the synthesis of 5-HTergic neurons [51], MAOA is a monoamine enzyme involved in neurotransmitter metabolism, and TPH2 acts as a key enzyme in 5-HT synthesis [16]. We found that ERα binds to the promoters of TPH2, MAOA, and PET1 and that ERβ binds to the promoter of MAOA. The discovery of these molecular targets and their applications in clinical settings are expected to overcome the side effects associated with oestrogen and SSRIs.

Part 3. ERs regulate the RNA and protein levels of TPH2 and MAOA and affect the mouse body temperature through the 5-HTergic neural pathway

In the present study, the body surface temperature of perimenopausal mice was measured in various regions. We found that the body temperature of the hairless tail and paws, which are the main heat sinks of mice, increased significantly after OVX, whereas the body temperature of the hair-coated head and back also increased but to a lesser extent. Considering these findings combined with the presence of 5-HT-positive neurons and 5-HT-related receptors in the hypothalamus, we speculated that the increase in the body surface temperature was a result of a decrease in the 5-HT content due to a decrease in the oestrogen levels after OVX. Negative feedback caused an increase in the expression of 5-HT-related receptors in the POA, but the small amount of 5-HT present could not fully activate

the 5-HT-related receptors and caused 5-HT-related receptor dysfunction. A higher basal body temperature is the underlying cause of perimenopausal hot flashes. The level of 5-HT in the brain in the presence of 5-HT1AR and 5-HT2AR determines the extent to which the body temperature is altered. The injection of 5-HT into the lateral ventricle increases the body temperature; similar to the clinical 5-HT syndrome produced by SSRI overuse, 5-HT-related receptors in the brain become overactivated due to a higher 5-HT content in the synaptic gap, and this overactivation subsequently leads to an increased body temperature. In contrast, after OVX, the amount of 5-HT produced in neurons is reduced, and negative feedback causes increases in the 5-HT1AR and 5-HT2AR levels. However, low levels of 5-HT are not sufficient to activate 5-HT-related receptors in the brain, resulting in abnormal heat dissipation and production, which manifests as an elevated body temperature. In the present study, ERα and ERβ depressors were injected into the RN of mice in the Sham group, which resulted in a decrease in the 5-HT level but no changes in the levels of 5-HT1AR or 5-HT2AR in the brain. Furthermore, 5-HT-related receptors in the brain are not sufficiently activated, and 5-HT1AR was preferentially activated, resulting in body heat dissipation and a reduced body temperature. The injection of activors of ERα and ERβ into the RN of mice in the OVX group resulted in an increase in the 5-HT levels in the brain. However, the levels of 5-HT1AR and 5-HT2AR were already increased due to negative feedback resulting from the long-term decrease in the 5-HT content, and the new increase in the 5-HT content in the brain was not sufficient to fully activate 5-HT-related receptors in the brain. In both experimental models, 5-HT-related receptors in the brain were underactivated, and the mice showed stronger reactions to increased 5-HT1AR levels, including enhanced heat dissipation and decreased body temperature.

However, we did not test other behavioural paradigms, mainly for the following reasons. First, regarding neuropsychiatric symptoms in perimenopause syndrome, Minami et al. researched memory impairment and depression in ovariectomized rats [52], and some research groups have explored OVX-induced anxiety-like behaviours [38,53,54]. Second, the effects of oestrogen receptor agonists or depressors on neuropsychiatric symptoms have also been studied [24,55]. Third, hot flashes are a specific symptom of menopause, with an incidence of 75% [3]. For the above mentioned reasons, our group focused on temperature regulation and thermoregulation-related behaviours.

Limitations: The present study showed that the hypoestrogenic state after OVX alters 5-HT-related receptor expression in the brain by affecting the levels of the ligand 5-HT. Previous studies have suggested that oestrogen receptors are widely distributed in the brain and may directly affect neurons in various brain regions, for example, by inducing ferroptosis [56] and neuroinflammatory responses [57]. From the current CUT&Tag results, it is possible that 5-HT2AR may be transcriptionally regulated by ERα and ERβ (data not shown), although this has not been validated at the cellular and animal levels. Additionally, apart from ERs, both 5-HT1AR and 5-HT2AR may also undergo transcriptional regulation by other transcription factors [58,59]. Therefore, the effect of oestrogen on 5-HTergic neural pathways and related physiological functions in the brain is the result of crosstalk among multiple factors.

The present study revealed the changes in the expression of 5-HTergic neural pathways (5-HT, 5-HT1AR and 5-HT2AR) in the brains of female mice after OVX and elucidated the possible mechanisms underlying these changes. We found that oestrogen-related receptors (ERα and ERβ) affect the expression of 5-HT metabolism-related enzymes. ERα- and ERβ-binding sites in the genome were identified by CUT&Tag profiling, and the positive effects of ERα and ERβ on TPH2 and MAOA transcription were further confirmed in SY5Y cells by dual-luciferase reporter assays. However, the RN is a brain region that contains several types of neurons, including 5-HTergic neurons, dopaminergic neurons, GABAergic neurons, and glutamatergic neurons [60]. Whether oestrogen-related receptors affect the metabolism of all of these neurotransmitters in the RN is worthy of further exploration. In subsequent research, we will analyse the possible effects of ERs on the transcription and translation of downstream RNAs by combining transcriptomics and CUT&Tag.

Conclusion: This study revealed the changes in 5-HT neuropathways (5-HT, 5-HT1AR and 5-HT2AR) in perimenopausal mice, mainly in brain regions related to regulation of the body temperature, mood, sleep and memory. This study clarified that the expression of oestrogen receptor decreased in perimenopause, which regulated the transcription levels of TPH2 and MAOA, and ultimately led to the reduction of 5-HT content, providing a new target for clinical diagnosis and treatment of perimenopausal diseases.

Funding

This research was supported by the Beijing Natural Science Foundation (7232091) and the National Natural Science Foundation of China (82171635).

Ethics statement

The animal experiments were approved by the Laboratory Animal Welfare Ethics Branch, Biomedical Ethics Committee, Peking University. Approval number: LA2022429.

Data availability statement

Part of the data are listed in the supplementary materials. More data will be provide available upon request.

CRediT authorship contribution statement

Hanfei Wang: Writing – review & editing, Writing – original draft, Visualization, Validation, Software, Project administration, Methodology, Investigation, Formal analysis, Data curation, Conceptualization. **Yanrong Sun:** Writing – review & editing, Software,

Resources, Methodology, Investigation, Formal analysis. **Wenjuan Wang:** Writing – review & editing, Software, Methodology, Formal analysis, Conceptualization. **Xiangqiu Wang:** Writing – original draft, Methodology, Formal analysis. **Jinglin Zhang:** Software, Methodology, Formal analysis, Data curation. **Yu Bai:** Methodology, Formal analysis. **Ke Wang:** Validation, Supervision, Project administration, Methodology. **Liju Luan:** Writing – review & editing, Supervision, Resources, Conceptualization. **Junhao Yan:** Writing – review & editing, Validation, Supervision, Project administration, Formal analysis. **Lihua Qin:** Writing – review & editing, Visualization, Supervision, Resources, Project administration, Funding acquisition, Formal analysis, Data curation, Conceptualization.

Declaration of competing interest

The authors declare that they have no known competing financial interests or personal relationships that could have appeared to influence the work reported in this paper.

Acknowledgements

We thank Furui Runze Company for the technical support provided; Transgene Company, XiaoChun Wang, and Haiyue Yu for the technical guidance with the qPCR assay; Vazyme Company, Caixin Zhen for the technical guidance with CUT&Tag; and Novogene Company, Chen Wang and Peking University, Donglin Yu for the help with the bioinformatic analysis of the results.

Appendix A. Supplementary data

Supplementary data to this article can be found online at https://doi.org/10.1016/j.heliyon.2024.e27976.

References

[1] V. Talaulikar, Menopause transition: physiology and symptoms, Best Pract. Res. Clin. Obstet. Gynaecol. 81 (2022) 3–7.
[2] R.A. Lobo, A. Gompel, Management of menopause: a view towards prevention, Lancet Diabetes Endocrinol. 10 (2022) 457–470.
[3] C.J. Crandall, J.M. Mehta, J.E. Manson, Management of menopausal symptoms: a review, JAMA 329 (2023) 405–420.
[4] M.A. Horowitz, D. Taylor, Tapering of SSRI treatment to mitigate withdrawal symptoms, Lancet Psychiatr. 6 (2019) 538–546.
[5] N. Leaf, HRT for treating menopause: known unknowns, Bmj 381 (2023) p1364.
[6] G.A. Petroianu, Hyperthermia and serotonin: the quest for a "better cyproheptadine", Int. J. Mol. Sci. 23 (2022).
[7] I.P. Voronova, 5-HT receptors and temperature homeostasis, Biomolecules 11 (2021).
[8] W. Wang, G. Cui, B. Jin, K. Wang, X. Chen, Y. Sun, et al., Estradiol Valerate and Remifemin ameliorate ovariectomy-induced decrease in a serotonin dorsal raphe-preoptic hypothalamus pathway in rats, Ann. Anat. 208 (2016) 31–39.
[9] N.K. Popova, A.S. Tsybko, V.S. Naumenko, The implication of 5-HT receptor family members in aggression, depression and suicide: similarity and difference, Int. J. Mol. Sci. 23 (2022).
[10] J. Kaufman, C. DeLorenzo, S. Choudhury, R.V. Parsey, The 5-ht1a receptor in major depressive disorder, Eur. Neuropsychopharmacol 26 (2016) 397–410.
[11] K.T. Kimura, H. Asada, A. Inoue, F. Kadji, D. Im, C. Mori, et al., Structures of the 5-HT(2A) receptor in complex with the antipsychotics risperidone and zotepine, Nat. Struct. Mol. Biol. 26 (2019) 121–128.
[12] G. Oikonomou, M. Altermatt, R.W. Zhang, G.M. Coughlin, C. Montz, V. Gradinaru, et al., The serotonergic raphe promote sleep in zebrafish and mice, Neuron 103 (2019) 686–701.
[13] M.S. Whitney, A.M. Shemery, A.M. Yaw, L.J. Donovan, J.D. Glass, E.S. Deneris, Adult brain serotonin deficiency causes hyperactivity, circadian disruption, and elimination of siestas, J. Neurosci. 36 (2016) 9828–9842.
[14] J.M. Monti, D. Monti, Role of dorsal raphe nucleus serotonin 5-HT1A receptor in the regulation of REM sleep, Life Sci. 66 (2000) 1999–2012.
[15] J.M. Monti, Serotonin control of sleep-wake behavior, Sleep Med. Rev. 15 (2011) 269–281.
[16] M. Goulty, G. Botton-Amiot, E. Rosato, S.G. Sprecher, R. Feuda, The monoaminergic system is a bilaterian innovation, Nat. Commun. 14 (2023) 3284.
[17] S.P. Fernandez, A. Muzerelle, S. Scotto-Lomassese, J. Barik, A. Gruart, J.M. Delgado-Garcia, et al., Constitutive and acquired serotonin deficiency alters memory and hippocampal synaptic plasticity, Neuropsychopharmacology 42 (2017) 512–523.
[18] Z.R. Shapiro, S. Cerasiello, L. Hartshorne, M.S. Matell, 5-HT1a receptor involvement in temporal memory and the response to temporal ambiguity, Front. Neurosci. 12 (2018) 439.
[19] M.V. King, C.A. Marsden, K.C. Fone, A role for the 5-HT(1A), 5-HT4 and 5-HT6 receptors in learning and memory, Trends Pharmacol. Sci. 29 (2008) 482–492.
[20] M. Luo, J. Zhou, Z. Liu, Reward processing by the dorsal raphe nucleus: 5-HT and beyond, Learn. Mem. 22 (2015) 452–460.
[21] J. Ren, A. Isakova, D. Friedmann, J. Zeng, S.M. Grutzner, A. Pun, et al., Single-cell transcriptomes and whole-brain projections of serotonin neurons in the mouse dorsal and median raphe nuclei, Elife 8 (2019).
[22] B.W. Okaty, K.G. Commons, S.M. Dymecki, Embracing diversity in the 5-HT neuronal system, Nat. Rev. Neurosci. 20 (2019) 397–424.
[23] S. Maioli, K. Leander, P. Nilsson, I. Nalvarte, Estrogen receptors and the aging brain, Essays Biochem. 65 (2021) 913–925.
[24] N. Donner, R.J. Handa, Estrogen receptor beta regulates the expression of tryptophan-hydroxylase 2 mRNA within serotonergic neurons of the rat dorsal raphe nuclei, Neuroscience 163 (2009) 705–718.
[25] R. Hiroi, R.J. Handa, Estrogen receptor-beta regulates human tryptophan hydroxylase-2 through an estrogen response element in the 5' untranslated region, J. Neurochem. 127 (2013) 487–495.
[26] Y. Sun, L.H. Qin, X. Chen, X. Yan, L. Mao, W. Bai, et al., Effects of black cohosh and estrogen on core body and tail-skin temperatures in ovariectomized rats by telemetric monitoring with dual thermistor probes, Climacteric 21 (2018) 153–159.
[27] P.J. Shughrue, M.V. Lane, I. Merchenthaler, Comparative distribution of estrogen receptor-alpha and -beta mRNA in the rat central nervous system, J. Comp. Neurol. 388 (1997) 507–525.
[28] A. Muzerelle, S. Scotto-Lomassese, J.F. Bernard, M. Soiza-Reilly, P. Gaspar, Conditional anterograde tracing reveals distinct targeting of individual serotonin cell groups (B5-B9) to the forebrain and brainstem, Brain Struct. Funct. 221 (2016) 535–561.
[29] G.F.K. Paxinos, The Mouse Brain in Stereotaxic Coordinates, Academic Press, San Diego, 2013.
[30] Y. Ma, M. Liu, L. Yang, L. Zhang, H. Guo, P. Qin, et al., Loss of estrogen efficacy against Hippocampus damage in long-term OVX mice is related to the reduction of Hippocampus local estrogen production and estrogen receptor degradation, Mol. Neurobiol. 57 (2020) 3540–3551.
[31] N.M. Barnes, T. Sharp, A review of central 5-HT receptors and their function, Neuropharmacology 38 (1999) 1083–1152.

[32] A. Ju, B. Fernandez-Arroyo, Y. Wu, D. Jacky, A. Beyeler, Expression of serotonin 1A and 2A receptors in molecular- and projection-defined neurons of the mouse insular cortex, Mol. Brain 13 (2020) 99.
[33] R.L. Carhart-Harris, D.J. Nutt, Serotonin and brain function: a tale of two receptors, J. Psychopharmacol. 31 (2017) 1091–1120.
[34] M. Cyr, M. Landry, T. Di Paolo, Modulation by estrogen-receptor directed drugs of 5-hydroxytryptamine-2A receptors in rat brain, Neuropsychopharmacology 23 (2000) 69–78.
[35] D. Winkler, E. Pjrek, S. Kasper, Anger attacks in depression–evidence for a male depressive syndrome, Psychother. Psychosom. 74 (2005) 303–307.
[36] J. Ren, D. Friedmann, J. Xiong, C.D. Liu, B.R. Ferguson, T. Weerakkody, et al., Anatomically defined and functionally distinct dorsal raphe serotonin sub-systems, Cell 175 (2018) 472–487.
[37] B. Yu, Q. Zhang, L. Lin, X. Zhou, W. Ma, S. Wen, et al., Molecular and cellular evolution of the amygdala across species analyzed by single-nucleus transcriptome profiling, Cell Discov 9 (2023) 19.
[38] Y. Wang, Y. Liu, J. Xiong, T. Di, Z. Yuan, J. Wu, et al., Reduced serotonin impairs long-term depression in basolateral amygdala complex and causes anxiety-like behaviors in a mouse model of perimenopause, Exp. Neurol. 321 (2019) 113030.
[39] B.A. Samuels, C. Anacker, A. Hu, M.R. Levinstein, A. Pickenhagen, T. Tsetsenis, et al., 5-HT1A receptors on mature dentate gyrus granule cells are critical for the antidepressant response, Nat. Neurosci. 18 (2015) 1606–1616.
[40] J. Zhang, C.Y. Cai, H.Y. Wu, L.J. Zhu, C.X. Luo, D.Y. Zhu, CREB-mediated synaptogenesis and neurogenesis is crucial for the role of 5-HT1a receptors in modulating anxiety behaviors, Sci. Rep. 6 (2016) 29551.
[41] M. Wang, H.F. Zong, K.W. Chang, H. Han, R.M. Yasir, N.S. Iffat, et al., 5-HT(1A)R alleviates Abeta-induced cognitive decline and neuroinflammation through crosstalk with NF-kappaB pathway in mice, Int. Immunopharm. 82 (2020) 106354.
[42] J. Wang, Y. Mei, X. Zhang, X. Wei, Y. Zhang, D. Wang, et al., Aberrant serotonergic signaling contributes to the hyperexcitability of CA1 pyramidal neurons in a mouse model of Alzheimer's disease, Cell Rep. 42 (2023) 112152.
[43] N.V. Weisstaub, M. Zhou, A. Lira, E. Lambe, J. Gonzalez-Maeso, J.P. Hornung, et al., Cortical 5-HT2A receptor signaling modulates anxiety-like behaviors in mice, Science 313 (2006) 536–540.
[44] J.M. Monti, H. Jantos, Differential effects of the 5-HT1A receptor agonist flesinoxan given locally or systemically on REM sleep in the rat, Eur. J. Pharmacol. 478 (2003) 121–130.
[45] J.M. Monti, D. Monti, Role of dorsal raphe nucleus serotonin 5-HT1A receptor in the regulation of REM sleep, Life Sci. 66 (2000) 1999–2012.
[46] H. Ma, L. Gu, Y. Wang, Q. Xu, Y. Zhang, W. Shao, et al., The states of different 5-HT receptors located in the dorsal raphe nucleus are crucial for regulating the awakening during general anesthesia, Mol. Neurobiol. 60 (2023) 6931–6948.
[47] R. Rothhaas, S. Chung, Role of the preoptic area in sleep and thermoregulation, Front. Neurosci. 15 (2021) 664781.
[48] S.W. Mitra, E. Hoskin, J. Yudkovitz, L. Pear, H.A. Wilkinson, S. Hayashi, et al., Immunolocalization of estrogen receptor beta in the mouse brain: comparison with estrogen receptor alpha, Endocrinology 144 (2003) 2055–2067.
[49] J. Zhang, W. Bai, W. Wang, H. Jiang, B. Jin, Y. Liu, et al., Mechanisms underlying alterations in norepinephrine levels in the locus coeruleus of ovariectomized rats: modulation by estradiol valerate and black cohosh, Neuroscience 354 (2017) 110–121.
[50] Q. Yang, Y. Sun, W. Wang, J. Jia, W. Bai, K. Wang, et al., Transient receptor potential melastatin 2 thermosensitive neurons in the preoptic area involved in menopausal hot flashes in ovariectomized mice, Neuroendocrinology 112 (2022) 649–665.
[51] B.W. Okaty, N. Sturrock, L.Y. Escobedo, Y. Chang, R.A. Senft, K.A. Lyon, et al., A single-cell transcriptomic and anatomic atlas of mouse dorsal raphe Pet1 neurons, Elife 9 (2020).
[52] A. Minami, H. Matsushita, D. Ieno, Y. Matsuda, Y. Horii, A. Ishii, et al., Improvement of neurological disorders in postmenopausal model rats by administration of royal jelly, Climacteric 19 (2016) 568–573.
[53] Y. Fang, J. Zhang, S. Zhu, M. He, S. Ma, Q. Jia, et al., Berberine ameliorates ovariectomy-induced anxiety-like behaviors by enrichment in equol generating gut microbiota, Pharmacol. Res. 165 (2021) 105439.
[54] R. Hiroi, R.A. McDevitt, J.F. Neumaier, Estrogen selectively increases tryptophan hydroxylase-2 mRNA expression in distinct subregions of rat midbrain raphe nucleus: association between gene expression and anxiety behavior in the open field, Biol. Psychiatr. 60 (2006) 288–295.
[55] C.K. Miller, J. Meitzen, No detectable changes in anxiety-related and locomotor behaviors in adult ovariectomized female rats exposed to estradiol, the ERbeta agonist DPN or the ERalpha agonist PPT, Horm. Behav. 152 (2023) 105363.
[56] Y. Tian, Y. Xie, Z. Guo, P. Feng, Y. You, Q. Yu, 17 beta-oestradiol inhibits ferroptosis in the hippocampus by upregulating DHODH and further improves memory decline after ovariectomy, Redox Biol. 62 (2023) 102708.
[57] T.E. Branyan, J. Aleksa, E. Lepe, K. Kosel, F. Sohrabji, The aging ovary impairs acute stroke outcomes, J. Neuroinflammation 20 (2023) 159.
[58] P.R. Albert, Transcriptional regulation of the 5-HT1A receptor: implications for mental illness, Philos. Trans. R. Soc. Lond. B Biol. Sci. 367 (2012) 2402–2415.
[59] M. Toth, Transcriptional regulation of the 5-HT2A receptor, Behav. Brain Res. 73 (1996) 183–186.
[60] K.W. Huang, N.E. Ochandarena, A.C. Philson, M. Hyun, J.E. Birnbaum, M. Cicconet, et al., Molecular and anatomical organization of the dorsal raphe nucleus, Elife 8 (2019).
[61] L. Lundholm, G. Bryzgalova, H. Gao, N. Portwood, S. Falt, K.D. Berndt, et al., The estrogen receptor alpha-selective agonist propyl pyrazole triol improves glucose tolerance in ob/ob mice; potential molecular mechanisms, J. Endocrinol. 199 (2008) X1.
[62] H.M. Weir, R.H. Bradbury, M. Lawson, A.A. Rabow, D. Buttar, R.J. Callis, et al., AZD9496: an oral estrogen receptor inhibitor that blocks the growth of ER-positive and ESR1-mutant breast tumors in preclinical models, Cancer Res. 76 (2016) 3307–3318.
[63] W. Tao, Y. Dong, Q. Su, H. Wang, Y. Chen, W. Xue, et al., Liquiritigenin reverses depression-like behavior in unpredictable chronic mild stress-induced mice by regulating PI3K/Akt/mTOR mediated BDNF/TrkB pathway, Behav. Brain Res. 308 (2016) 177–186.